PONTIFICIA UNIVERSIDAD CATÓLICA DE CHILE
SCHOOL OF ENGINEERING

SVD-BASED BEAMFORMING COMMUNICATIONS OVER NARROW-BAND QUASI-STATIC MIMO CHANNELS

FELIPE KETTLUN

Thesis submitted to the Office of Research and Graduate Studies
in partial fulfillment of the requirements for the degree of
Master of Science in Engineering

Advisor:
CHRISTIAN OBERLI

Santiago de Chile, August 2014

PONTIFICIA UNIVERSIDAD CATÓLICA DE CHILE
SCHOOL OF ENGINEERING

SVD-BASED BEAMFORMING COMMUNICATIONS OVER NARROW-BAND QUASI-STATIC MIMO CHANNELS

FELIPE KETTLUN

Members of the Committee:
CHRISTIAN OBERLI
MARCELO GUARINI
JAIME ANGUITA
YADRAN ETEROVIC

Thesis submitted to the Office of Research and Graduate Studies
in partial fulfillment of the requirements for the degree of
Master of Science in Engineering

Santiago de Chile, August 2014

The empires of the future
are the empires of the mind.
WINSTON CHURCHILL

ACKNOWLEDGEMENTS

First I would like to thank my advisor, Professor Christian Oberli, for believing in my abilities and always being available to answer my questions and give me his advise on the several technical problems faced during this process.

Moreover, I also want to thank all the people I have worked with during the last year: Joaquín Aldunate, Santiago Barros, Jean Paul de Villers-Grandchamps, Carlos Feres, Marcelo Guarini, Diego Kaulen, Fernando Rosas and Joaquín Venegas. I have learned a lot from each of them.

I would like to thank CONICYT Chile for supporting this research with the scholarship CONICYT-PCHA Magíster Nacional 2013-221320215 and the project CONICYT FONDEF D09I1094 under which this thesis was developed.

Finally, I want to thank my family and friends for all the support they have given me throughout these years.

TABLE OF CONTENTS

LIST OF FIGURES

LIST OF TABLES

ABSTRACT

Improving the reliability of a wireless communication system, by using joint transmit and receive diversity over multiple-input multiple-output (MIMO) channels, requires configuring the antenna array radiation pattern. To maximize the signal-to-noise ratio (SNR), the transmission has to be precoded and decoded with the respective first singular vectors, given by the Singular Value Decomposition (SVD) of the MIMO channel matrix. This technique, referred to as SVD-based beamforming, has two main challenges: It requires channel state information at the transmitter (CSIT) and the computation load required to calculate the SVD of a channel matrix is generally inviable for low-power consumption devices.

In this thesis, we propose a method that, instead of relying on feeding back actual channel or SVD coefficients to the transmitter, takes advantage of channel reciprocity between transmitter and receiver to acquire the precoding vector at the transmitter. The presented algorithm consists of three stages: a first forward preamble transmission ("*Ping*") used for channel training, then a backward response ("*Pong*") for channel-dependent reverse channel training, and finally a forward *Payload* transmission which carries the actual payload data. Instead of computing the full SVD, the presented method only requires a low-complexity iteration algorithm to calculate the first singular vector for performing the beamforming.

The present thesis also studies link acquisition and hardware architecture considerations for the digital implementation of the proposed algorithm. Particularly, the method is simulated with the specifications of the testbed developed at the Wireless Technologies Laboratory (LATINA, by its Spanish acronym) of *Pontificia Universidad Católica de Chile* (UC). The results show that the proposed algorithm approaches the theoretical bit error rate (BER) of the SVD-based beamforming.

Keywords: MIMO, SVD, beamforming, CSI, eigenchannel, channel reciprocity.

RESUMEN

Mejorar la confiabilidad de un sistema de comunicaciones inalámbricas, usando diversidad de transmisión y recepción en canales de múltiple entrada y múltiple salida (MIMO), implica configurar los patrones de radiación de los arreglos de antenas. Para maximizar la razón señal a ruido (SNR), la transmisión tiene que ser precodificada y decodificada con los vectores singulares primarios, dados por la descomposición de valor singular (SVD) de la matriz de canal MIMO. Esta técnica, llamada *beamforming* SVD, enfrenta dos grandes desafíos: necesita información del estado del canal en el transmisor (CSIT) y la carga computacional para obtener la SVD de la matriz de canal es generalmente inviable para dispositivos de bajo consumo energético.

En esta tesis se desarrolla una técnica que, en lugar de realimentar hacia el transmisor los coeficientes de la matriz de canal o los de la SVD, aprovecha la reciprocidad del canal entre el transmisor y el receptor para adquirir el vector de precodificación en el transmisor. El método contempla tres etapas: una primera transmisión de preámbulo ("*Ping*") usada para entrenamiento de canal, una respuesta de vuelta dependiente del canal ("*Pong*") para entrenamiento inverso, y, finalmente, una transmisión *Payload* hacia el receptor con los datos a comunicar. En vez de calcular la SVD completa, el método presentado sólo necesita de un algoritmo iterativo de baja complejidad, para calcular el primer vector singular necesario para realizar *beamforming*.

Esta tesis también estudia consideraciones de adquisición del enlace y arquitectura de *hardware* para la implementación digital del algoritmo propuesto. Particularmente, el método es simulado con las especificaciones de la plataforma experimental desarrollada en el Laboratorio de Tecnologías Inalámbricas (LATINA) de la Pontificia Universidad Católica de Chile (UC). Los resultados muestran que el algoritmo propuesto se acerca a la tasa de error de bit (BER) teórica del *beamforming* SVD.

Palabras Claves: MIMO, SVD, *beamforming*, CSI, canal propio, reciprocidad de canal.

1. INTRODUCTION

Multiple-input multiple-output (MIMO) techniques have become one of the most important concepts in the development of new wireless communication systems. The use of multiple antennas allows for manipulating the signals transmitted or received on each antenna of a node in order to achieve a better performance than a single-input single-output (SISO) system. MIMO can be used to improve the reliability of reception (diversity gain) or to increase the data rate (multiplexing gain) (Goldsmith, 2005).

The diversity gain is obtained by using the redundancy of multiple antennas, i.e. conditioning the signals in order to combine them constructively at the receiver. Conversely, the full multiplexing gain is obtained when each antenna of the transmitter sends independent information. The aired signals superimpose over the air, in such a manner that each receiving antenna acquires a linear combination of the sent data. Therefore, it is required that the receiver is able to separate again such information.

The majority of the research and developments of new technologies have been concentrated on achieving multiplexing gain due to the increasing demand for higher data rates. This focus has led to new standards of communication, such as IEEE 802.11n (Wi-Fi), Worldwide Interoperability for Microwave Access (WiMAX) and Long Term Evolution (LTE) (Sibille, Oestges, & Zanella, 2010). Still, application fields exist in which the paradigm is not a limited data rate, but a limited energy budget. Wireless sensor network (WSN) is an example of these type of applications, in which a set of electronic devices communicate with each other wirelessly in a coordinated manner to sense variables of a given environment such as temperature, pressure, humidity, etc.

Recently, several scholars have proposed the use of MIMO communications as an alternative for WSN to become more efficient in their energy use (Liu, Li, & Chen, 2005; Rosas & Oberli, 2012a; S., Goldsmith, & Bahai, 2004). This means that it is possible to reach longer distances per wireless hop with the same power, or vice versa, use less power to reach the same distances. One of the toughest restrictions of WSN devices is the power

they consume. WSN have to be designed to not require external power connection, and also to last for long periods of time without any assistance. Hence, WSN designs tend to seek low-complexity implementation, which limits the range of the communication. Because the power needed by current WSN devices demands large batteries, it is not yet economically feasible to cover large areas with the technology, leaving the area of communications of low-data rate and long distances still to be developed (Saito, Kagami, Umehira, & Kado, 2008). This area of wireless communications receives the name of wide area ubiquitous network (WAUN), and its position in term of the coverage range and data rate is depicted in Fig. 1.1.

This thesis was developed in the context of the project FONDEF D09I1094: Wireless sensor networks with multiple antenna technologies, which was carried out by the Wireless Technologies Laboratory (LATINA, by its Spanish acronym) of *Pontificia Universidad Católica de Chile* (UC). The project addresses the design and development of a digital wireless system for WSN applications using multiple antennas both at transmitter and receiver.

1.1 Motivation and Research Problem

In every digital wireless system the receiver has to perform several tasks to recompose the message sent over the air by the transmitter. These necessary tasks tackle the several obstacles imposed by the physical medium and by the physical impairments in the transceivers. The main adversities are:

- Uncertainty of the presence of a signal in the air and its timing.
- Signal degradation by path loss and channel dispersion.
- Thermal noise from the receiver's front-end components.
- Carrier frequency offset (CFO) produced by mismatches in oscillator frequencies in the down-conversion from radio frequency (RF) to baseband.

Resolving the sent message at the receiver requires to solve successfully all the previous issues. The biggest challenge exists at the beginning of every new transmission, when

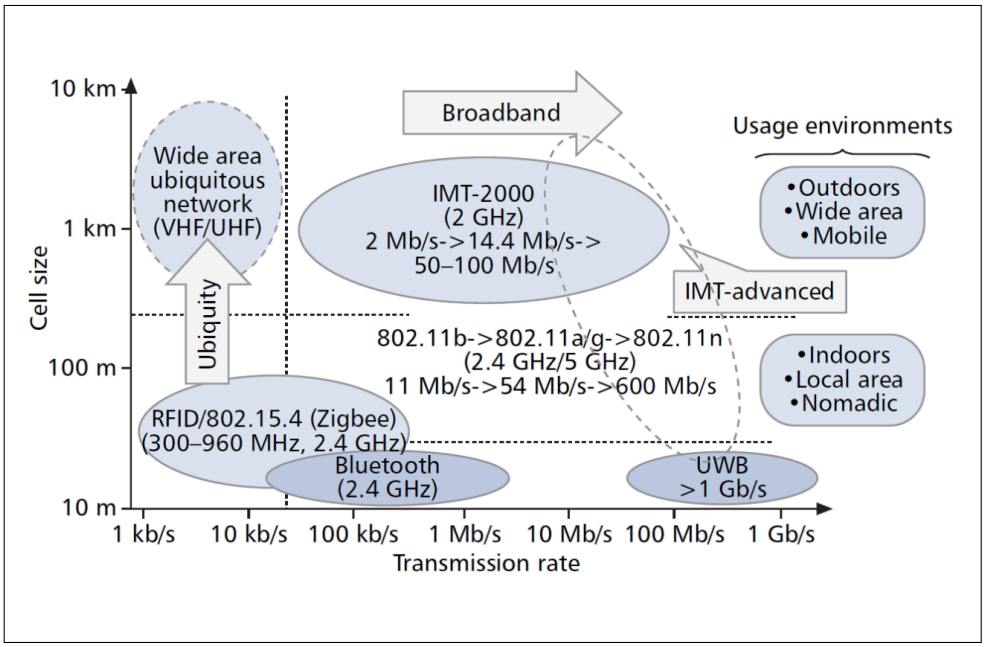

FIGURE 1.1. Technical trends of various wireless systems and where the WAUN is positioned (Saito et al., 2008).

.

the signal in the air must be first detected and then symbol timing, coarse CFO and channel state information (CSI) must be estimated. This stage is commonly known as *acquisition*. After this phase, and as long as the transmission lasts, the receiver must adapt to changes in the propagation environment and correct for time variations, phase known as *tracking*.

In SISO systems, even if the receiver can correct all the previous impairments, there is no guarantee that the error probability of the established link will be low enough. The possibility that the channel can be in a deep fading during the transmission is the main obstacle for a communication without errors.

In narrow-band quasi-static channels, a solution to improve the performance is to make the same information to pass through different propagation paths, each with independent fading, such that the communication can remain reliable as long as one of the paths is strong enough. These independent channels can be obtained by the use of multiple antennas at the transmitter and/or receiver, where each pair of transmit and receive antenna corresponds to an individual propagation path.

There exist several schemes for multiple antennas that achieve diversity gain, such as equal gain combining (EGC), maximal-ratio combining (MRC) and space-time block coding (STBC). Nevertheless, the highest diversity degree can only be achieved using the strongest eigenmode of the MIMO channel (Goldsmith, 2005). This technique consists of using the principal right and principal left singular vectors of the MIMO channel matrix as beamformers at the transmitter and receiver respectively. The two main drawbacks of this approach are: it requires channel state information (CSI) at both sides of the communication link and it needs to determine the aforementioned vectors, which may be computationally expensive (Goldsmith, 2005; Tse & Viswanath, 2005).

In this context, the work presented here proposes a set of low-complexity techniques to set up the strongest eigenmode between two nodes in narrow-band quasi-static MIMO channels. The techniques allow for acquiring the singular vectors at the transmit and receive side by using channel training in both directions, but without requiring full CSI at the transmitter. For the training, this work assumes channel reciprocity between the forward and backward transmissions between the two nodes. Even though non-symmetric characteristics of the RF electronic circuitry break this property, there exist various solutions to this problem. Some of them rely on hardware techniques and other on calibration algorithms (Guillaud, Slock, & Knopp, 2005; Jungnickel, Kruger, Istoc, Haustein, & Von Helmolt, 2004). Addressing the implementation of these methods is beyond the scope of this work, and is assumed to be adequately solved.

1.2 Research Goals and Contributions

The main goal of this thesis is to develop low-complexity techniques to establish a reliable wireless communication over narrow-band quasi-static MIMO channels. In order to achieve this, the present work is structured around the following specific goals:

1. To develop a low-complexity narrow-band MIMO communication scheme that achieves the diversity gain of the strongest eigenmode.

2. To study link acquisition considerations. This comprises the design of appropriates preambles to perform signal synchronization (packet detection, timing recovery and CFO correction), and the study of the performance loss due to imperfect CSI.
3. To study the proposed scheme under real implementation considerations, and adjust it accordingly. This includes determining the appropriate transceiver architecture and designing a fast and low-complexity automatic gain control (AGC) loop to adjust the strength of the narrow-band signal at the receiver.
4. To develop a complete communication simulator with the same specifications of the LATINA UC testbed, in order to obtain results of the performance of the proposed algorithms.

The main contribution of the present work is to present a new method for establishing a reliable wireless link with MIMO technology while addressing the implementation difficulties associated with this method. This is a remarkable contribution for applications that require low-power consumption and low-data rate, such as WSN.

1.3 Thesis Structure

Chapter 2 introduces the main concepts and design challenges to achieve diversity gain in MIMO digital wireless communication systems, particularly for SVD-based beamforming. It also presents considerations for implementing a real communication system. These considerations allow to introduce the testbed developed at LATINA UC, whose specifications are used in this thesis for validating the results. Chapter 3 provides a literature review on the prior art concerning SVD-based communication and on the corresponding implementation considerations for MIMO systems.

Chapter 4 develops a novel low-complexity scheme, the Ping-Pong-Payload (PPP), for establishing a MIMO communication with the highest diversity gain, by using the strongest eigenchannel. Chapter 5 examines some considerations for implementing this scheme in a real digital wireless system. The considerations include, synchronization

of the received signal, channel estimation and the design of a fast and low-complexity AGC for the LATINA UC testbed. With the architecture specifications, simulations are conducted to obtain performance results of the PPP. Finally, Chapter 6 draws the main conclusions and suggests future research.

2. SVD-BASED COMMUNICATIONS

This chapter provides a brief tutorial on the theoretical models used for the communications over wireless channels and presents the necessary considerations for implementing a real communication system.

2.1 Communication Model

Wireless digital communications encode information into a carrier signal which is then transmitted over a wireless channel. Usually, the channel deteriorates the signal in such a way that the received wave has to be processed in order to extract the data. However, in some environments, this processing may not be sufficient for successful detection of the information. Therefore, diversity gain must be used to improve the performance of the system. One of the forms of obtaining such diversity is by using multiple antennas. Although several schemes exist that utilize multiple antennas, only Singular Value Decomposition beamforming (SVD-BF) achieves the minimal error rate.

2.1.1 Digital Modulation

The basic principle of passband digital modulation is to encode an information bit stream into a carrier signal which is then transmitted over a communications channel. In general, modulated carrier signals encode information in the amplitude $\xi(t)$, frequency $f(t)$, or phase $\delta(t)$ of a carrier signal of frequency f_c (Goldsmith, 2005). Thus, the modulated signal can be represented as

$$\begin{aligned} s(t) &= \xi(t)\sqrt{2}\cos\left[2\pi(f_\mathrm{c} + f(t))t + \delta(t) + \phi_0\right] \\ &= \xi(t)\sqrt{2}\cos\left[2\pi f_\mathrm{c} t + \phi(t) + \phi_0\right] \quad , \end{aligned} \tag{2.1}$$

where $\phi(t) = 2\pi f(t)t + \delta(t)$ and ϕ_0 is the phase offset of the carrier. This representation combines frequency and phase modulation into angle modulation.

We can rewrite (2.1) in terms of its in-phase and quadrature components as

$$s(t) = \sqrt{2}s_{\mathrm{I}}(t)\cos(2\pi f_{\mathrm{c}}t) - \sqrt{2}s_{\mathrm{Q}}(t)\sin(2\pi f_{\mathrm{c}}t) \quad , \tag{2.2}$$

where $s_{\mathrm{I}}(t) = \xi(t)\cos\phi(t)$ and $s_{\mathrm{Q}}(t) = \xi(t)\sin\phi(t)$ are called, respectively, the in-phase and the quadrature components of $s(t)$.

The complex baseband representation of $s(t)$ is

$$s(t) = \Re\{\sqrt{2}s_{\mathrm{BB}}(t)e^{j2\pi f_{\mathrm{c}}t}\} \quad , \tag{2.3}$$

where $s_{\mathrm{BB}}(t) = s_{\mathrm{I}}(t) + js_{\mathrm{Q}}(t)$ is the complex envelope of $s(t)$. This representation is useful since receivers typically process the in-phase and quadrature signal components separately.

In linear modulations, the information bit stream is encoded in the amplitude and/or phase of the signal $s_{\mathrm{BB}}(t)$ over a time interval of T_{s}, such as

$$s_{\mathrm{BB}}(t) = s_{\mathrm{I}}(t) + js_{\mathrm{Q}}(t) = (x_{\mathrm{I}} + jx_{\mathrm{Q}})\, g(t) \qquad 0 \leq t \leq T_{\mathrm{s}} \quad , \tag{2.4}$$

where $x_{\mathrm{I}} \in \mathbb{R}$ and $x_{\mathrm{Q}} \in \mathbb{R}$ are the in-phase and quadrature components of a certain message and $g(t)$ is a fixed shaping pulse of bandwidth B_{I}. The constellation point $x = x_{\mathrm{I}} + jx_{\mathrm{Q}} = (x_{\mathrm{I}}, x_{\mathrm{Q}})$ is called *symbol*. A set of M symbols can represent a sequence of $\log_2 M$ bits. T_{s} is the symbol time, which defines the data rate $\frac{\log_2 M}{T_{\mathrm{s}}}$. Without loss of generality, we will assume throughout this work that the energy of x is unitary, i.e. $|x|^2 = 1$.

In this thesis, quadrature phase-shift keying (QPSK) modulations are utilized, for reasons that will be explained in Chapter 4. Fig. 2.1 depicts the corresponding symbol constellation for QPSK.

2.1.2 Wireless Channel

The wireless channel is a medium where a wavefront between a transmitter and a receiver follows multiple paths (Fig. 2.2). On each of these tracks, the signal is affected

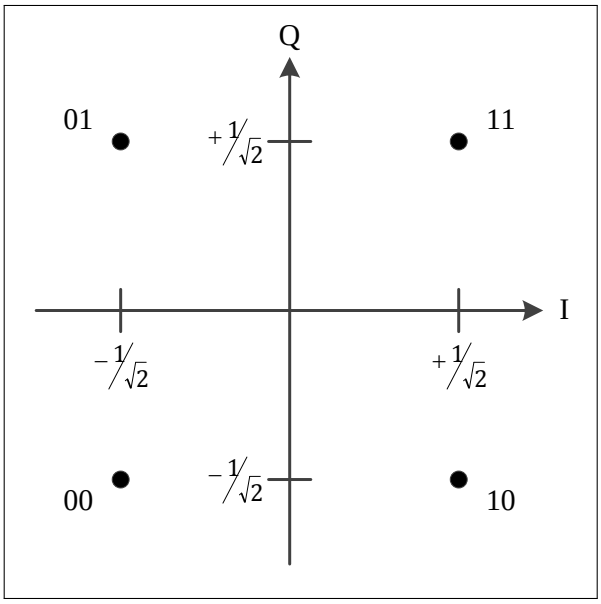

FIGURE 2.1. QPSK modulation utilizes 4 points on the constellation diagram, equispaced around a circle. This structure allows to encode 2 bits per symbol. To minimize the BER, the bits are assigned using Gray coding. It is to note that the energy of each symbol is unitary.

by reflection, refraction, diffraction, absorption, polarization and scattering (Paris, 1969). Important to note is that the distortion the signal suffers is independent on each path.

The transmitted signal is affected by three main factors: path loss between transmitter and receiver, small-scale fading in the local area of the receiver and thermal noise at the front-end of the receiver. The baseband-equivalent of the received signal is

$$r_{\text{BB}}(t) = \sqrt{E_{\text{s}}} \sum_{k=0}^{K(t)} h_k(t) s_{\text{BB}}(t - \tau_k(t)) + n_{\text{BB}}(t) \ , \tag{2.5}$$

where E_{s} corresponds to the average received signal energy per symbol. The received energy depends on the power gain of the antennas at both transmitter and receiver, the transmitted wavelength, the distance, and the path loss exponent of the medium. The term $\sum_{k=0}^{K(t)} h_k(t) s_{\text{BB}}(t - \tau_k(t))$ corresponds to the sum of the line-of-sight (LOS) path ($k = 0$) and all resolvable multipath components ($k \geq 1$), where $K(t) \in \mathbb{N}$ is the number of multipath components, $\tau_k(t) \in \mathbb{R}$ the delay of path k and $h_k(t) \in \mathbb{C}$ the respective phase

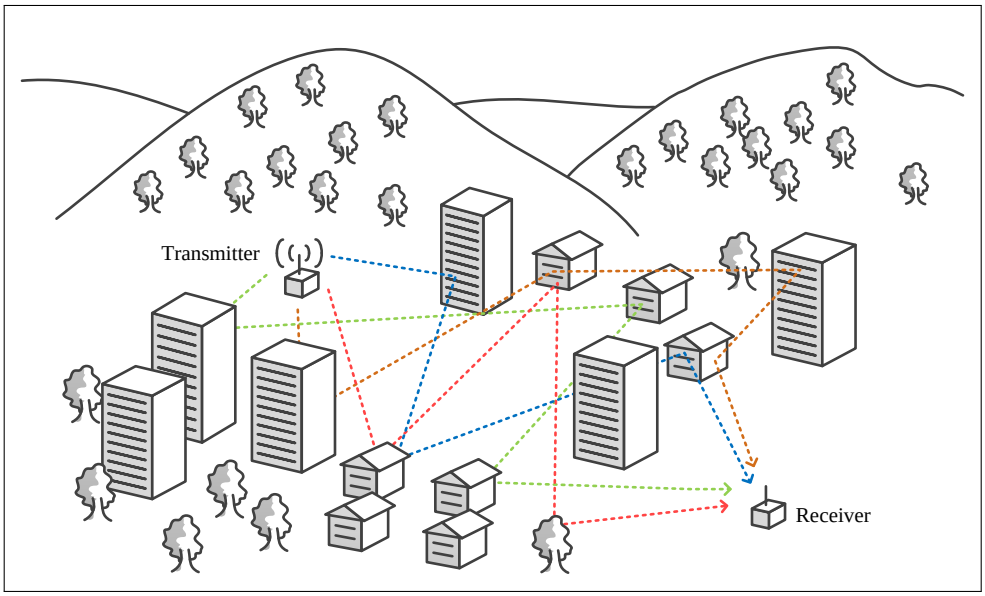

FIGURE 2.2. Representation of a transmitted wavefront facing several obstacles. (Feres, 2013)

shift and amplitude gain. And finally, $n_{\text{BB}}(t)$ is the complex baseband-equivalent additive white Gaussian noise (AWGN) within the bandwidth B_{I} of the signal, with i.i.d. zero mean and $\nu^2 = \frac{N_0}{2} 2B_{\text{I}}$ variance, where $\frac{N_0}{2}$ is the power spectral density of the noise. This noise is generated by thermal agitation of the electrons of the conductor (Goldsmith, 2005).

In narrow-band channels, the delay spread is small relative to the inverse signal bandwidth B_{I}. Thus, it can be assumed that $s_{\text{BB}}(t - \tau_k) \approx s_{\text{BB}}(t) \ \forall k$. The received signal can then be rewritten as

$$\begin{aligned} r_{\text{BB}}(t) &= \sqrt{E_{\text{s}}} \left(\sum_{k=0}^{K(t)} h_k(t) \right) s_{\text{BB}}(t) + n_{\text{BB}}(t) \\ &= \sqrt{E_{\text{s}}} h(t) s_{\text{BB}}(t) + n_{\text{BB}}(t) \ , \end{aligned} \tag{2.6}$$

where $h(t) \in \mathbb{C}$ represents the overall channel effect, and can be separated in an in-phase and a quadrature component as $h(t) = h_{\text{I}}(t) + j h_{\text{Q}}(t)$. Since the channel can be considered as stationary and ergodic and if $K(t)$ is large, which in practice occurs, the

Central Limit Theorem can be used to approximate $h_{\mathrm{I}}(t)$ and $h_{\mathrm{Q}}(t)$ as jointly Gaussian random processes (Goldsmith, 2005).

Coherence time is defined as the time duration over which the channel response is considered to not change significantly. This time depends on the mobility of the environment. In a quasi-static channel, also called slow-fading channel, the total time of the communication is smaller than the coherence time. Thereafter the channel response can be assumed to be the same over time, i.e. $h(t) \approx h$. Thus, the received signal formulation can be reduced to

$$r_{\mathrm{BB}}(t) = \sqrt{E_{\mathrm{s}}} h s_{\mathrm{BB}}(t) + n_{\mathrm{BB}}(t) \ . \tag{2.7}$$

In digital communications, the probability of detection error is minimized by the receiver by declaring the received signal as the signal in the set of possible transmitted signals that is "closest" to the one received. This closeness analysis is simpler if signals are represented in a finite-dimensional vector space instead of a infinite dimensional function space. The finite-dimensional vector space is called the signal space.

$y = \int_0^{T_{\mathrm{s}}} r_{\mathrm{BB}}(t) g^{-1}(t)\,\mathrm{d}t$ and $n = \int_0^{T_{\mathrm{s}}} n_{\mathrm{BB}}(t) g^{-1}(t)\,\mathrm{d}t$ are the signal space representation of the received signal and AWGN, respectively, where $n \sim \mathcal{CN}(0, N_0)$. Recalling that $\int_0^{T_{\mathrm{s}}} x g(t) g^{-1}(t)\,\mathrm{d}t = x$, the signal space model for a narrow-band quasi-static channel is

$$y = \sqrt{E_{\mathrm{s}}} h x + n \ . \tag{2.8}$$

2.1.3 Rayleigh Fading and Diversity Gain

The most common way to measure the performance of a communication scheme is studying its probability of error. System designers are typically more interested in the bit error rate (BER), than in the symbol error rate (SER), since "bit errors drive the performance of higher layer networking protocols and end-to-end performance" (Goldsmith, 2005).

The probability of error for a given system depends on the SNR, which is defined as the ratio of the received signal power P_{r} to the power of the noise within the bandwidth B_{I} of the transmitted signal $s(t)$. The SNR γ corresponds then to

$$\gamma = \frac{P_{\mathrm{r}}}{N_0 B_{\mathrm{I}}} \ . \tag{2.9}$$

Considering that $|x|^2 = 1$ and taking (2.8), it can be observed that

$$P_r = \frac{\left|\sqrt{E_{\mathrm{s}}} h x\right|^2}{T_{\mathrm{s}}} = \frac{|h|^2 E_{\mathrm{s}}}{T_{\mathrm{s}}} \ . \tag{2.10}$$

The SNR is then expressed as

$$\gamma = \frac{|h|^2 E_s}{N_0 B_{\mathrm{I}} T_{\mathrm{s}}} = \frac{|h|^2 E_{\mathrm{b}} \log_2 M}{N_0 B_{\mathrm{I}} T_{\mathrm{s}}} \ , \tag{2.11}$$

where $E_{\mathrm{b}} = E_{\mathrm{s}} / \log_2 M$ is the average signal energy per bit.

Considering that for general pulses $B_{\mathrm{I}} = (1+\beta)/T_{\mathrm{s}}$ for some constant β (e.g. for raised cosine pulses, $0 \leq \beta \leq 1$), it can be obtained

$$\gamma = \frac{|h|^2}{(1+\beta)} \frac{E_{\mathrm{s}}}{N_0} = \frac{|h|^2 \log_2 M}{(1+\beta)} \frac{E_{\mathrm{b}}}{N_0} \ . \tag{2.12}$$

To represent the behavior of channel h, two main statistical models are commonly used: Rayleigh and Rician (Tse & Viswanath, 2005). If the multiple reflective paths are large in number and there is no LOS signal component, the envelope of the received signal is statistically described by a Rayleigh probability density function (pdf). On the other hand, when there is a dominant nonfading signal component present, such as a line-of-sight propagation path, the small scale fading envelope is described by a Rician pdf (Sklar, 1997).

In this thesis, the Rayleigh fading channel model is preferred as it represents the most adverse scenario (Haustein et al., 2001). Thereafter, a communication system should meet

performance specifications in any Rician channel if it already complies the requirements for the Rayleigh case. The Rayleigh fading model states that $h \sim \mathcal{CN}(0,1)$, such that $\mathbb{E}\left\{|h|^2\right\} = 1$ (Tse & Viswanath, 2005), where $\mathbb{E}\{\cdot\}$ denotes the expected value operator.

Fig. 2.3 depicts the communication BER of an ideal AWGN channel, i.e. $h = 1$, and of a Rayleigh fading channel. Although channel knowledge is available at the receiver, the Rayleigh communication has a mediocre performance compared to the AWGN one. The main reason is that there is a significant probability that the channel is in a "deep fade" (Tse & Viswanath, 2005).

A solution to improve the performance is to make the same information to pass through different signal paths, each with independent fading. The result is that the communication is reliable as long as one of the paths is strong enough. There are several ways to obtain diversity between two nodes:

- **Time**: The information can be dispersed in different coherence periods if the coherence time is shorter than the communication time.
- **Frequency**: The information can be dispersed by transmitting the same narrowband signal at different carrier frequencies, where the carriers are separated by the coherence bandwidth of the channel.
- **Space**: Using multiple transmit or receive antennas spaced sufficiently.
- **Polarization**: Using the different polarizations (vertical/horizontal) of the electromagnetic waves.

Time diversity is generally not possible in quasi-static channels, due to the transmitted packet lasts much shorter than the coherence time. Frequency diversity requires the overall bandwidth to be wider than the required to transmit the same information using a single carrier frequency. It also usually requires additional transmit power to send the signal over multiple frequency bands (Goldsmith, 2005). Polarization diversity does not allow to use more than two channels and their level of correlation is usually higher than the other types of diversity forms (Bensky, 2004). This thesis seeks to achieve diversity gain by the use of space.

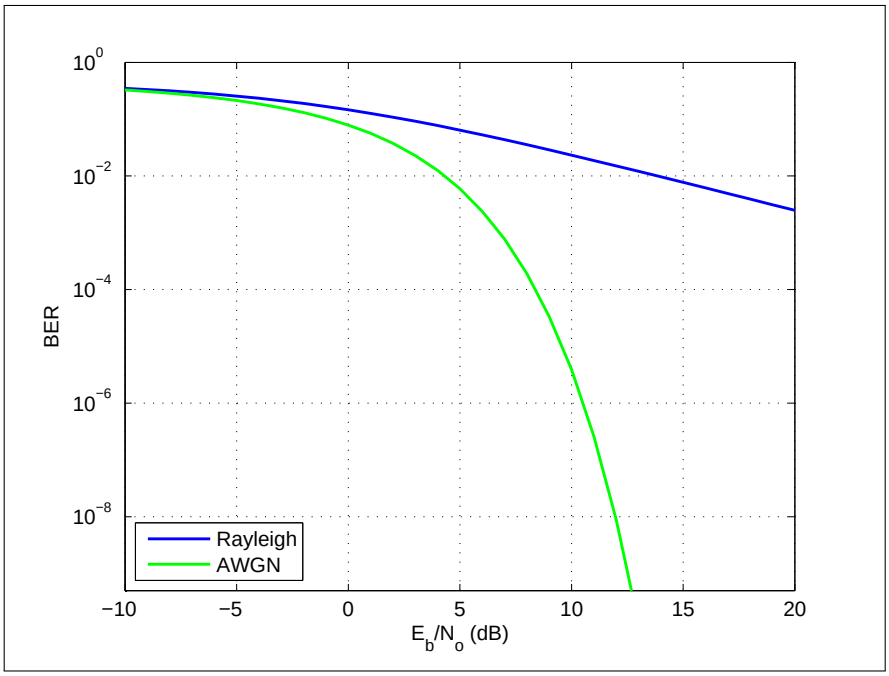

FIGURE 2.3. BER for Rayleigh and AWGN channel.

2.1.4 SVD-based Beamforming

MIMO communications consider the use of multiple antennas at both the transmitter and receiver to improve the performance. In the present work, a MIMO system with N_{t} transmit antennas and N_{r} receive antennas can be modeled just by extending (2.8), such that

$$\mathbf{y} = \sqrt{E_{\mathrm{s}}}\mathbf{H}\mathbf{x} + \mathbf{n} \ , \tag{2.13}$$

where column vector $\mathbf{x} \in \mathbb{C}^{N_{\mathrm{t}}}$ represents the transmitted symbols, $\mathbf{y} \in \mathbb{C}^{N_{\mathrm{r}}}$ is the column vector of received symbols, $\mathbf{n} \in \mathbb{C}^{N_r}$ is the complex AWGN column vector with i.i.d. zero mean and $\nu^2 = N_0$ variance elements, and $\mathbf{H} \in \mathbb{C}^{N_{\mathrm{r}} \times N_{\mathrm{t}}}$ is the matrix of Rayleigh channel gains $h_{i,j}$ representing the complex gain from transmit antenna j to receive antenna i. The elements $h_{i,j}$ are assumed to be i.i.d. circularly symmetrical complex Gaussian random variables, with zero mean and unit variance. To maintain the average signal energy, the restriction $||\mathbf{x}|| = 1$ is imposed, where $||\cdot||$ denotes the Euclidean norm.

Just to simplify the analysis, the following model for the MIMO communication is rather used

$$\mathbf{y} = \mathbf{H}\mathbf{x} + \mathbf{n} \ , \tag{2.14}$$

where the only difference respect to (2.13) is that the elements of the complex AWGN vector $\mathbf{n}$ have $\nu^2 = \frac{N_0}{E_\mathrm{s}}$ variance.

The MIMO channel can be decomposed via the singular value decomposition (SVD) into parallel independent channels if there is channel state information (CSI) at both transmitter and receiver (Goldsmith, 2005). The SVD theorem (Eckart & Young, 1939) states that for any matrix $\mathbf{H}$ there exists a factorization of the form

$$\mathbf{H} = \mathbf{U}\mathbf{\Sigma}\mathbf{V}^\dagger \ , \tag{2.15}$$

where $(\cdot)^\dagger$ denotes the conjugate transpose operator. $\mathbf{U} = [\mathbf{u}_1, \mathbf{u}_2, ..., \mathbf{u}_{N_\mathrm{r}}] \in \mathbb{C}^{N_\mathrm{r} \times N_\mathrm{r}}$ and $\mathbf{V} = [\mathbf{v}_1, \mathbf{v}_2, ..., \mathbf{v}_{N_\mathrm{t}}] \in \mathbb{C}^{N_\mathrm{t} \times N_\mathrm{t}}$ are unitary matrices, i.e. $\mathbf{U}\mathbf{U}^\dagger = \mathbf{I}_{N_\mathrm{r}}$, $\mathbf{V}\mathbf{V}^\dagger = \mathbf{I}_{N_\mathrm{t}}$, being $\mathbf{I}_N$ the identity matrix of size $N \times N$. Singular vectors $\mathbf{u}_k$ and $\mathbf{v}_k$ are not unique, since $\{e^{j\theta}\mathbf{u}_k\}_{k=1}^{N_\mathrm{r}}$ and $\{e^{j\theta}\mathbf{v}_k\}_{k=1}^{N_\mathrm{t}}$ are also sets of singular vectors for $\mathbf{H}$, for any arbitrary θ. The matrix $\mathbf{\Sigma}$ is a $N_\mathrm{r} \times N_\mathrm{t}$ diagonal matrix of non-negative real numbers σ_k such that $\sigma_1 \geq \sigma_2 \cdots \geq \sigma_{\mathrm{rank}(\mathbf{H})}$, where $\mathrm{rank}(\mathbf{H})$ is limited by the number of antennas at the transmitter and receiver as $\mathrm{rank}(\mathbf{H}) \leq \min(N_\mathrm{t}, N_\mathrm{r})$, and particularly for rich scattering environment $\mathrm{rank}(\mathbf{H}) = \min(N_\mathrm{t}, N_\mathrm{r})$ (Goldsmith, 2005).

MIMO diversity gain can be achieved by using the strongest eigenchannel, i.e. the best of the parallel independent channels, which is also commonly called singular value decomposition beamforming (SVD-BF). The technique consists of precoding with $\mathbf{v}_1$ the symbol $d \in \mathbb{C}$ to be transmitted and decoding with $\mathbf{u}_1^\dagger$ the received vector signal as

$$\begin{aligned}\mathbf{u}_1^\dagger \mathbf{y} &= \mathbf{u}_1^\dagger \left(\mathbf{H}\mathbf{v}_1 d + \mathbf{n}\right) \\ &= \mathbf{u}_1^\dagger \mathbf{U}\mathbf{\Sigma}\mathbf{V}^\dagger \mathbf{v}_1 d + \mathbf{u}_1^\dagger \mathbf{n} \ ,\end{aligned} \tag{2.16}$$

where $\tilde{y} = \mathbf{u}_1^\dagger \mathbf{y}$ is a scalar that corresponds to the received symbol d under thermal noise $\tilde{n} = \mathbf{u}_1^\dagger \mathbf{n}$, which has the same statistics of each element of $\mathbf{n}$ as $\mathbf{u}_1$ is a unit vector. By the SVD properties, the received symbol corresponds to

$$\tilde{y} = \sigma_1 d + \tilde{n} \ , \tag{2.17}$$

where the largest singular value σ_1 represents the equivalent SISO channel gain, which can be approximated by the gain of a Nakagami channel (Rosas & Oberli, 2013).

In addition to SVD-BF, several other schemes exist to improve BER by using multiple antennas at the receiver, at the transmitter or both. The most popular ones are EGC, MRC and STBC. Nonetheless, the optimal scheme for maximizing the SNR gain is to use the SVD-BF (Goldsmith, 2005), as it can be seen in Fig. 2.4. This technique achieves the highest diversity gain.

2.2 Real Communication Systems

In this section, some of the considerations needed for developing a real communication system are presented. They include link acquisition and hardware architecture considerations. Particularly, the testbed developed at LATINA UC, whose specifications are used in this thesis for performance validation, is presented.

2.2.1 Link Acquisition

Packet switching is the most common paradigm used in digital communications, for it allows a large number of data users to remain virtually connected to the same physical channel in the network. The technique breaks each message into smaller units. Each unit, called *packet*, contains not only the data but also certain amount of control information and

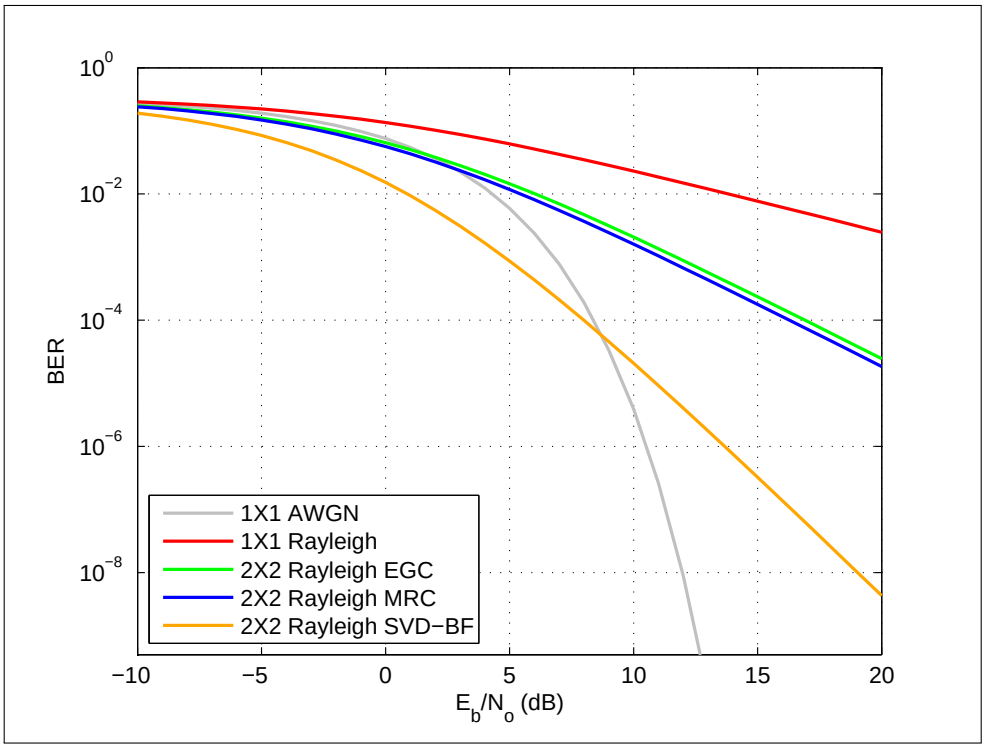

FIGURE 2.4. Theoretical BER of different MIMO schemes compared to the basic Rayleigh scenario. The best performance is achieved by SVD-BF, which even outperforms the AWGN channel in low E_{b}/N_0.

error recovery provisions (Rappaport, 2002). The typical structure of a packet is shown in Fig. 2.5.

Synchronous digital communications carry the information in uniformly spaced pulses and the received signal is completely known except for the data symbols and a group of variables called *reference parameters*: symbol timing, carrier frequency offset (CFO), sampling frequency offset (SFO) and CSI, among others. Only by exploiting the knowledge of these parameters an accurate replica of the transmitted data can be produced at the receiver (Mengali & D'Andrea, 1997). The largest uncertainty exists at the beginning of every new transmission, as none of these parameters is known. Discovering them receives the name of *acquisition*. The acquisition process can be divided into two main

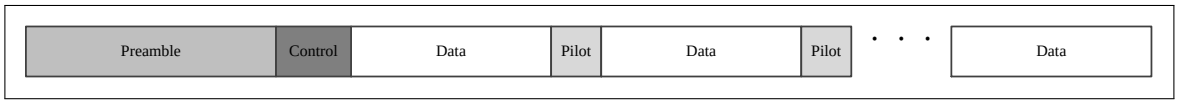

FIGURE 2.5. Representation of the general structure of a packet. The preamble is used for synchronization and channel estimation, both necessary to establish a reliable communication link. The control signal is intended for protocols, configuration settings and addressing. The pilots are utilized to maintain the link by adapting to the changes in the environment. Finally, the data corresponds to the actual information to be sent.

tasks: synchronization of the receiver with respect to the transmitter and channel estimation, necessary for correcting the distortions of phases and magnitudes contained in the incoming signal.

The first task a receiver has to resolve successfully in every new communication is the *packet detection*, which consists in continuously checking for the existence of a packet over the air and raising a flag when it detects one. The flag is used to start performing the acquisition tasks.

In a typical digital system the received waveform is first digitized with a sampling frequency N_{up} times higher than the symbol rate. Next, the digital signal is passed through a matched filter, whose output is sampled at the symbol rate. In order to accurately determine the transmitted data, the receiver has to acquire knowledge of the ideal sampling instants. The task of determining these instants is known as symbol timing acquisition.

The baseband signal must be recovered using local references with the same frequency f_{c} and phase ϕ as the incoming carrier. The local reference correspond to an electronic oscillator, which produces a sinusoidal voltage at a fixed frequency. Although all nodes in a network are designed to work at the same nominal frequency, they differ randomly from this reference due to differences in manufacturing processes, temperature, humidity, load impedance and components aging, among others (Walls & Vig, 1995). As all operations performed by the node are based on the oscillating frequency of the crystal on board, there might be SFO and CFO between two nodes. SFO affects mostly long and wideband

transmissions, and therefore it can be neglected for packet-switched narrow-band communications. Conversely, the CFO has two important consequences on the performance of the system. First, the spectrum of the baseband signal will not be centered respect to the matched filter. Hence, the correlation will not be maximal, which is equivalent to a loss in the SNR. The second effect is a rotation in the received symbol constellation, which increases the BER. Therefore, carrier synchronization is a vital task for correct detection.

In summary, a narrow-band receiver must perform the following tasks:

1. Packet detection
2. Symbol timing recovery
3. CFO correction

2.2.2 Transceiver Architecture

A transceiver comprises both a transmitter and a receiver. Each of these consist of two important parts: the frequency up or down-converter (RF module) and the baseband processing engine, as Fig. 2.6 shows. The first one converts the signal from a baseband frequency to the carrier frequency and vice versa and is usually analog because of the high signal frequencies involved. The baseband processing block performs the modulation and demodulation of a digital signal, whose frequency content is on the order of symbol rate. The digital processing allows for using more complex modulation schemes than what an analog signal processor does (Crols & Steyaert, 1998).

a) Baseband Processing

The modulation and demodulation occurs at the baseband modem of the transceiver shown in Fig. 2.7. The main task at the transmitter is to transform the bit sequences of information into symbols and thereafter pulse shape them with $g[k]$ so that the transmitted signal has a limited bandwidth. The opposite is done at the receiver, the received signal is matched filtered with $g^*[-k]$. With the correct timing, the data symbols can be extracted from this filtered signal and then be transformed into the corresponding bit sequence. The baseband modem also performs some tasks to synchronize the received signal.

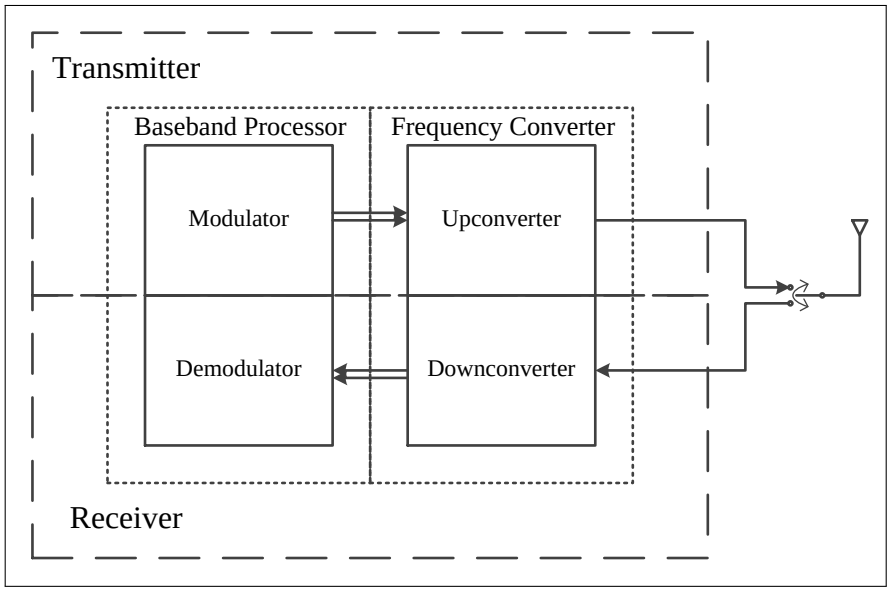

FIGURE 2.6. General structure of a typical transceiver. It comprises both the transmitter and receiver. At the same time it can be divided into the baseband processor and the frequency converter.

b) Frequency Conversion

The design specifications are more difficult to comply at the receiver than at the transmitter due to the thermal noise and eventual interference. Therefore, frequency conversion design is mostly driven by the downconversion.

There are two main downconversion architectures used in wireless communication systems: the heterodyne and the homodyne receiver. The heterodyne receiver downconverts the signal to an intermediate frequency (IF) signal, performs band-pass filtering and amplification, and translates the spectrum again, now to a zero frequency. Instead, the homodyne receiver downconverts the signal directly to zero frequency. For their spectral capabilities, they are also called, respectively, IF and zero-IF receiver (Crols & Steyaert, 1998).

The zero-IF receiver requires fewer components and is easier to implement than the IF receiver. Nevertheless, it has an important drawback with DC-offsets produced by the mixing of the local oscillator with its leakage signal (Razavi, 1998). This issue can be solved

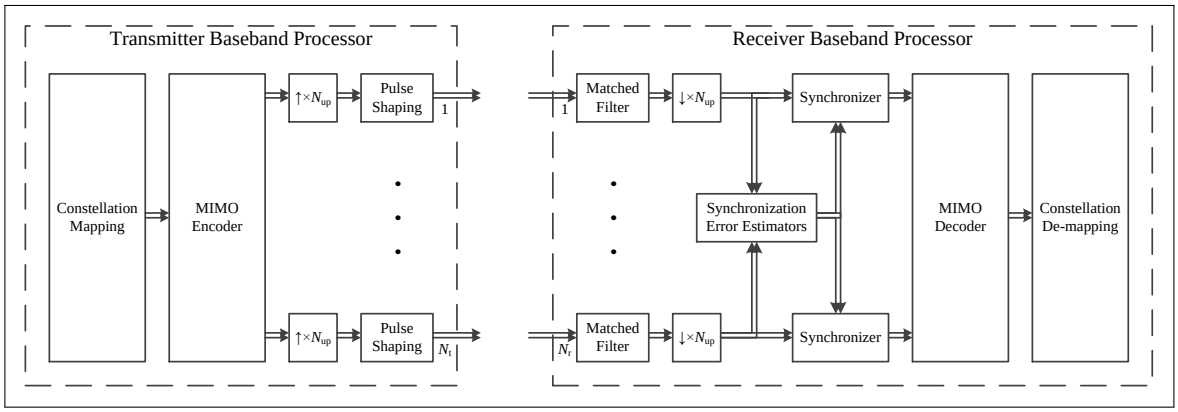

FIGURE 2.7. MIMO Baseband Processor with N_{t} transmit antennas and N_{r} receive antennas.

in the digital domain using a nonlinear scheme to determine the DC-level dynamically and feed it back into the analog part. However, the response of this scheme is limited by the low-pass filters (LPF) needed in the receiver. In narrow-band communications, these LPF have a bandwidth too small to make the settling time of the receiver short enough for the packet-switched scheme needed.

For the above reasons, an IF receiver is preferred for narrow-band communications. Furthermore, low-frequency operations, like the second set of mixing and filtering, can be performed more efficiently in the digital domain using so-called digital IF. Hence, the first IF signal is digitized with an analog-to-digital Converter (ADC). Thereafter, the digital signal is mixed with the quadrature phases of a digital sinusoid for the final downconversion to baseband. Finally, the output signals are low-pass filtered to provide the quadrature baseband signals. The architectures with digital IF at the receiver and at the transmitter are shown in Fig. 2.8.

The input signal to the ADC typically is no higher than a few hundred of microvolts. Its magnitude also oscillates depending mostly on the channel realization. In order to optimally utilize the dynamic range of the ADC, an AGC must be added to control the variable-gain amplifier (VGA).

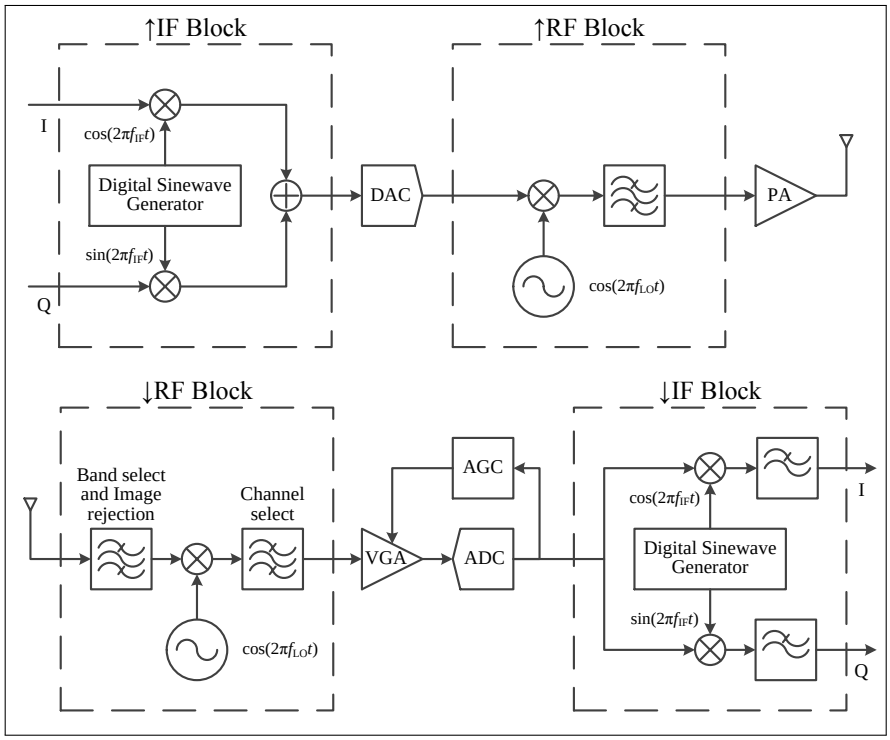

FIGURE 2.8. The upconverter (top) receives an in-phase and a quadrature digital signal. They are upconverted to the IF and mixed to transform them into a single analog wave. This signal is upconverted to the RF, whose power is amplified to finally be transmitted. The downconverter (bottom) filters the desired analog signal to downconvert it to the IF. This signal is digitized and then separated in its in-phase and quadrature waves.

2.2.3 Automatic Gain Control

The general function of any AGC is to automatically adjust the output signal of a VGA to an optimal rated level for different input signal strengths. This is required for it to assure that neither large signals are clipped nor the system's quantization noise grows above a tolerable level.

An AGC is implemented using a control loop structure that regulates the receiver's output level in a similar way as a voltage regulator maintains a constant output voltage. Generally, the envelope of the receiver's output is detected on the digital side of the ADC and compared to the desired level. This difference is used to change the VGA gain in the direction that reduces the error.

The main problem and challenge in any AGC design is the trade-off between the settling time and the stability of the loop. If the response is too fast (high loop bandwidth) the AGC could undesirably modify the modulation on the signal. On the contrary, if the response is too slow, information is lost until the gain is stabilized.

2.2.4 LATINA UC Testbed

The LATINA UC testbed operates in the industrial, scientific and medical (ISM) radio band, i.e. 902-928 MHz, with an IF of 6.75 Mhz. Each node of the testbed possesses 4 antennas. For simplicity, the following number of operating antennas are considered: $N_{\text{t}} = \{1, 2, 4\}$ and $N_{\text{r}} = \{1, 2, 4\}$.

The transmitter of the LATINA UC testbed (Fig. 2.9) works as explained below. In the Constellation Mapping block, each bit sequence to be sent is mapped to a symbol x, with its in-phase and quadrature components. The symbol is weighed on the different antennas by the MIMO encoder module according to the coefficients of the beamforming vector. On each transmit branch, the symbols are upsampled with zero stuffing by rate N_{BB} (i.e. $N_{\text{BB}} - 1$ zeros are inserted in between the symbols) and thereafter pulse shaped with $g[k]$. To achieve $N_{\text{up}} = N_{\text{IF}} N_{\text{BB}}$ samples per symbol a sinc interpolation is applied, where N_{IF} defines the IF. In each ↑IF module the received wave is upconverted to an IF signal for being transformed into an analog signal by the DAC. The analog signal is upconverted to the RF. Finally, the power amplifier gives the signal the transmit power.

In the receiver, depicted in Fig. 2.10, each antenna captures its own signal and down-converts it to an IF signal. A VGA at the entrance of the ADC adjusts the power of the signal in order to use the full resolution of the ADC. Next, the digital signal is sampled with a rate N_{up} times the symbol rate and downconverted to the zero frequency, yielding quadrature outputs. Because these outputs are limited in their frequency content by the LPF of the IF module, the signals can be downsampled, yielding N_{BB} samples per symbol.

The first task the receiver has to perform successfully in every new communication is to detect the presence of a packet. In order to accomplish that, the output signal of the

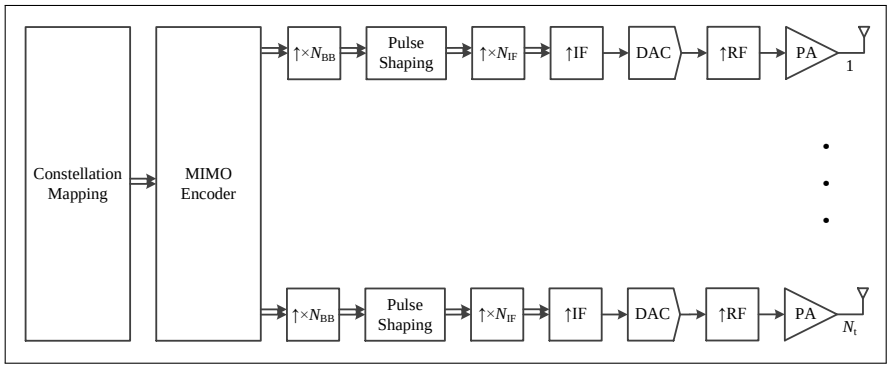

FIGURE 2.9. LATINA UC testbed transmitter overview.

downsampler is filtered with the matched filter and then decoded differentially to feed the Preamble Correlator block. The Packet Detector module recognizes when the magnitude of the correlation is higher than the given threshold λ_{PD} and raises the respective flag. The same output of the Preamble Correlator is used by the coarse CFO corrector.

The first set of registers, just following the downconversion from IF to baseband in Fig. 2.10, allows the CFO correction of the incoming signal considering the delay of the packet detection. Further downstream, the timing of the signals is corrected with an interpolation method, after which the oversampling is not necessary. The signals are compared to the stored preamble and pilots, to make a fine tuning of the CFO (Fine CFO Corrector block).

The symbols are fed into the MIMO decoder, where a channel estimation is performed so that the payload data following the preamble can be equalized correctly. Finally, the resulting symbol is fed into the Constellation De-mapping module to obtain the data bits.

The system operates with QPSK ($M = 4$) and with symbol rate of 13.2 kBd, resulting in a data rate of 26.4 kbps. Since $N_{\text{BB}} = 4$ (Feres, 2013), $N_{\text{IF}} = 512$ for achieving the IF of 6.75 MHz. An ADC operating at 27 MHz with 8 bits of resolution is included.

For the pulse shaping $g[k]$ a Square-Root Raised Cosine (SRRC) filter is used, with a group delay of 3 and $\beta = 0.5$. The impulse response of the filter is shown in Fig. 2.11. The corresponding bandwidth B_{I} is 19.78 kHz.

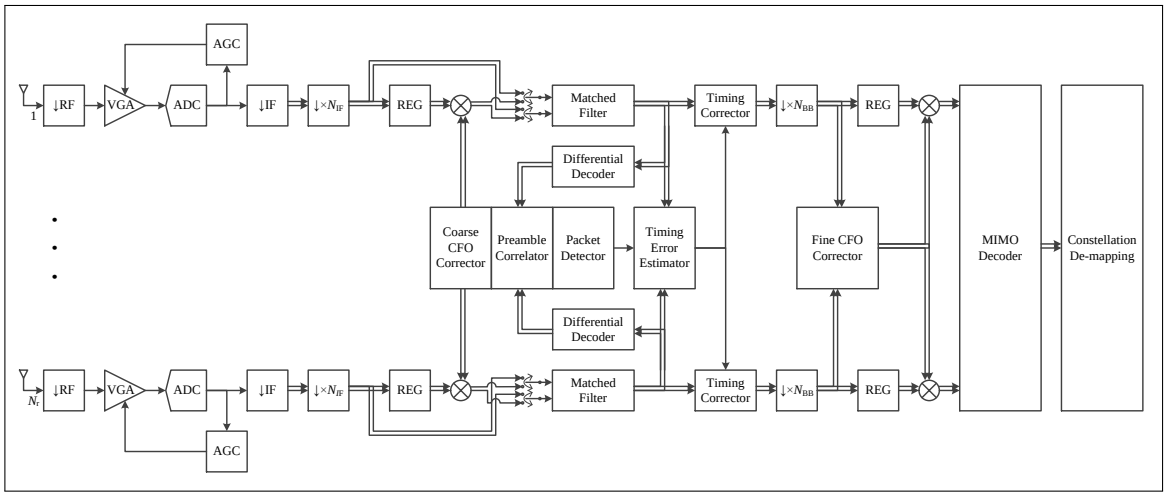

FIGURE 2.10. LATINA UC testbed receiver overview.

A summary of the specifications of the system can be found in Table 2.1.

TABLE 2.1. LATINA testbed specifications

Symbol	**Parameter**	**Value**
f_{c}	Carrier frequency	$915 - 930\,\mathrm{MHz}$
f_{IF}	Intermediate frequency	$6.75\,\mathrm{MHz}$
T_{s}	Symbol time	$75.86\,\mu\mathrm{s}$
B_{I}	In-band bandwidth	$19.78\,\mathrm{kHz}$
N_{t}	Number of transmit antennas	$\{1, 2, 4\}$
N_{r}	Number of receive antennas	$\{1, 2, 4\}$
N_{b}	ADC resolution	$8\,\mathrm{bits}$
N_{BB}	Baseband oversampling factor	4
N_{IF}	IF oversampling factor	512

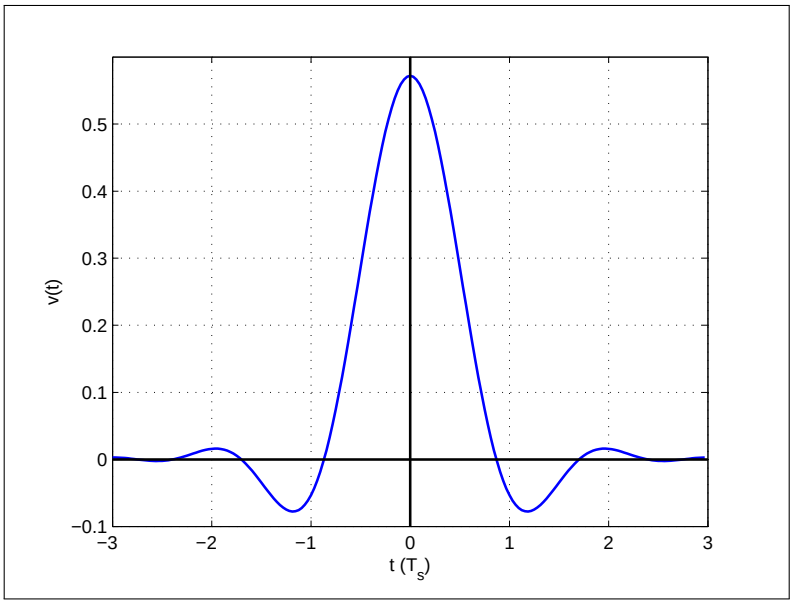

FIGURE 2.11. SRRC used in LATINA testbed. It considers a group delay of 3 and $\beta = 0.5$.

3. PRIOR ART

The following literature review summarizes the prior art on SVD-based beamforming and on the implementation considerations for MIMO systems that were presented in Chapter 2. It begins with SVD-based beamforming in Section 3.1, in which methods for feeding back CSI to the transmitter and for computing the SVD of the channel matrix are considered. Section 3.2 provides a review of the prior art on MIMO acquisition algorithms and chooses one that conforms to the specifications of this work. The literature also comprises AGC loops. This review focuses on digital architectures that can be adapted for the LATINA UC testbed.

3.1 On SVD-based Beamforming

In order to make use of the previously presented MIMO beamforming, vector $\mathbf{v}_1$ and $\mathbf{u}_1$ must be known at the transmitter and at the receiver, respectively.

Usually, channel state information at the receiver (CSIR) is acquired by sending known training symbols to the receiver (Hassibi & Hochwald, 2003). On the other hand, channel state information at the transmitter (CSIT) can be obtained by two different ways, depending upon the chosen duplexing scheme for the system.

For time-division duplex (TDD) systems CSIT can exploit the reciprocity of the channel. The property states that the channel responses in both directions are the same if the signals operate on the same frequency band. This is based on the property that electromagnetic waves in both directions go through the same physical perturbations, such as reflection and refraction (Smith, 2004). Channel reciprocity is modeled using $\mathbf{H}$ and $\mathbf{H}^T$ for the forward and backward transmission, respectively.

CSIT attainment in TDD systems considers a certain source device *I* sending a training signal to a destination device *II*, which estimates the channel coefficients. Then, an equivalent backward transmission is conducted within the coherence time and with the

same carrier frequency and bandwidth, so that I acquires CSI by reverse channel training (RCT) (Venkataramani & Marzetta, 2003).

For frequency-division duplex (FDD) systems, forward-link and backward-link portions of the bandwidth are apart enough to assume they are independent of each other. Thereby, channel reciprocity cannot be assumed. Instead, a dedicated feedback link is utilized. The disadvantage of this technique is that since the channel matrix $\mathbf{H}$ is in general estimated at the receiver, not at the transmitter, it requires the full matrix $\mathbf{H}$ to be transmitted at full precision back to the transmitter on some return channel. This usually involves an unacceptable overhead. To reduce the feedback, only a permissible set of precoding matrices may be utilized. The selection of the matrix is performed at the receiver following channel estimation, and the index of the optimum matrix within the codebook is then signaled back to the transmitter, incurring a much-reduced overhead. To reduce the feedback even more, some solutions signal back only the index of the beamforming vector instead of the index of the channel matrix (Love, Heath, & Strohmer, 2003; Mukkavilli, Sabharwal, Erkip, & Aazhang, 2003; Narula, Lopez, Trott, & Wornell, 1998; Xia & Giannakis, 2006). This approach is used in most of the recent and emerging MIMO wireless standards, such as WiMAX, 3GPP-LTE and LTE-Advanced (Sibille et al., 2010).

Although CSIT can be attained, communication over the strongest singular mode is seldom used, as calculating the SVD of the MIMO channel matrix, in order to obtain the beamforming vectors, is computationally costly. Much research has been done to find techniques for reduced complexity SVD computation (Studer, Blosch, Friedli, & Burg, 2007; Zhan, Chen, & Wu, 2012), but the propositions so far are still inadequate for implementation in systems with a restricted energy budget. The development of stable and efficient algorithms for computing the SVD is a challenging task. The first solutions were proposed just in the sixties (Golub & Kahan, 1965). Although nowadays various methods for performing the SVD exist, the Golub-Reinsch algorithm (GRA) (Golub & Reinsch, 1970) is the most utilized for arbitrary matrices because of its numerical stability, reduced computational cost and good convergence velocity (Björck, 1996).

The GRA, as most of the SVD algorithms, calculate all the singular vectors. To calculate only the first singular vectors, either the left or right one, the power iteration algorithm (PIA) is the preferred solution (Golub & Van Loan, 1996).

To overcome the SVD computation complexity, some algorithms, that take advantage of the reciprocity of the channel, have been proposed (Dahl, Christophersen, & Gesbert, 2004; Gazor & AlSuhaili, 2010; Tang, Vucetic, & Li, 2005; Xia, Niu, Oh, & Ngo, 2008). These algorithms implement the PIA, but requiring neither channel estimate nor vector computation. By operating on the same frequency band in both directions, the channel itself performs the PIA via forth and back transmissions.

In Tang et al. (2005) an iterative scheme for direct estimation of the best singular vector at both sides of the wireless link is proposed. A random unit vector is sent from the source. Then, the destination side normalizes, conjugates and retransmits the received vector signal without any additional precoding back to the original transmitter. This one in turn also normalizes, conjugates and retransmits the received signal back again. By repeating these iterations, the received vector on each side converges toward the required singular vector for the beamforming, i.e. the precoding vector at the transmitter and the decoding one at the receiver. Once the training stage has been achieved, the payload data can be sent. This iterative scheme is represented in Fig. 3.1.

Dahl et al. (2004) develops the Blind Iterative MIMO Algorithm (BIMA). Unlike the former one by Tang et al. (2005), Dahl's does not require a training stage. The decisions about the received symbols are used as if they were training symbols. The beamforming vectors are initialized as random vectors and are updated in each transmission, converging toward the singular vectors required for the beamforming. Xia et al. (2008) go further, by extending this method to orthogonal frequency-division multiplexing (OFDM). The drawback of these algorithms is their slow convergence, requiring many transmissions to achieve an acceptable BER. Their performance in low SNR scenarios is also poor (Gazor & AlSuhaili, 2010).

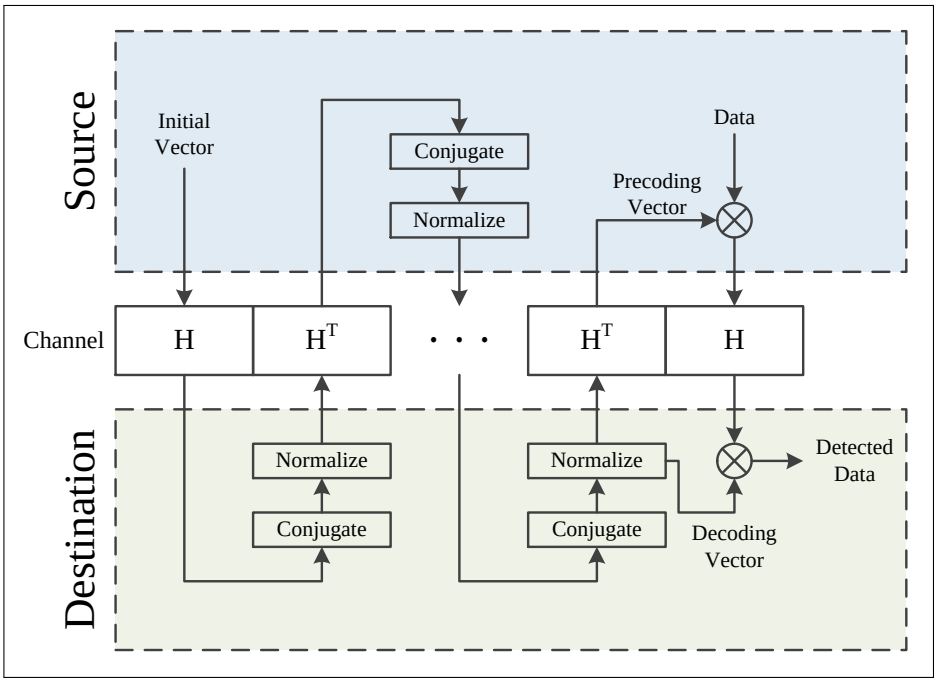

FIGURE 3.1. Representation of the iterative scheme proposed by Tang et al. (2005).

To improve performance at low SNRs, Gazor and AlSuhaili (2010) extend BIMA proposing an adaptive algorithm, which estimates the principal singular vectors at both sides using a weighted sum of previous estimates and the current received signal. Despite reducing significantly the effect of the noise, the convergence of the algorithm is still slow. Hence, the algorithm is not a good solution for intermittent transmissions or when only one of the nodes sends payload data.

This work proposes an algorithm which requires channel estimation, as most of the commercial technologies, but which takes advantage of channel reciprocity for setting up the communications over the strongest eigenchannel in only three low-complexity steps. The novel scheme is presented in Chapter 4.

3.2 On Implementation Considerations for MIMO Systems

3.2.1 MIMO Acquisition Algorithm

Several algorithms exist that address the problem of synchronization in MIMO channels. Because this task must be performed both fast and accurately, only training assisted methods are considered (Besson & Stoica, 2003; Czylwik, 1999; Perels, Studer, & Fichtner, 2007; Simoens & Moeneclaey, 2006), because blind approaches do not provide good enough results for packet-switched communications. Furthermore, most of the training-based algorithms tackle each of the synchronization tasks independently or are developed for wide-band systems, like orthogonal frequency-division multiplexing (OFDM) (Schellmann, Jungnickel, & Von Helmolt, 2005) and direct-sequence spread spectrum (DSSS) (Nagaraj, Khan, Schlegel, & Burnashev, 2006).

The algorithm proposed by Feres (2013) is a joint solution to the problems of packet detection, coarse symbol timing recovery and coarse CFO correction for narrow-band MIMO channels. The algorithm takes advantage of MIMO diversity to improve its performance.

Feres (2013) proposes a staggered sequence preamble (Fig. 3.2), whereby each antenna j transmits $\frac{L_\mathrm{p}}{N_\mathrm{t}}$ symbols of a sequence $\mathbf{p} \in \mathbb{C}^{L_\mathrm{p}}$. These symbols result from differentially encoding a source sequence $\tilde{\mathbf{p}}$. The l-th symbol to be transmitted over the air is attained as

$$p_l = p_{l-1}\tilde{p}_l \ , \tag{3.1}$$

where $\tilde{p}_l$ is the l-th symbol of the preamble in the non-differential domain.

At the receiver, on each antenna i, at the sample k, the matched filtered signals $y_i[k]$ are differentially decoded as

$$\bar{y}_i[k] = y_i[k]y_i[k - N_\mathrm{BB}]^* \ , \tag{3.2}$$

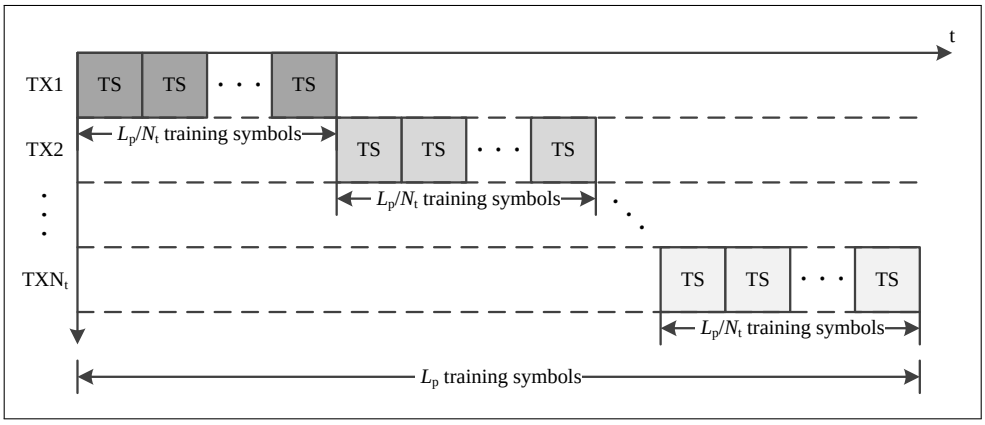

FIGURE 3.2. Staggered preamble where each block represents a training symbol (L_p in total).

where k corresponds to the sample time. This differential signal is summed over all the received antennas and correlated with the non-differential preamble as

$$R[k] = \frac{1}{L_\mathrm{p} N_\mathrm{r}} \sum_{l=1}^{L_\mathrm{p}} \sum_{i=1}^{N_\mathrm{r}} \bar{y}_i[k - L_\mathrm{p} + l] \tilde{p}_n^* \ . \tag{3.3}$$

At the precise moment $k = L_\mathrm{p}$ when the received symbols are totally aligned with their respective coefficients of the correlation, its value is

$$R[L_\mathrm{p}] = \frac{E_s}{N_\mathrm{r} N_\mathrm{t}} e^{j2\pi \Delta f T_\mathrm{s}} \sum_{i=1}^{N_\mathrm{r}} \sum_{j=1}^{N_\mathrm{t}} |h_{i,j}|^2 + n_\mathrm{R}[L_\mathrm{p}] \ , \tag{3.4}$$

where Δf is the CFO and $n_\mathrm{R}[L_\mathrm{p}]$ is the equivalent AWGN after the correlation process.

For packet detection the metric $|R[k]|^2$ is used for its property of having a low value except at the precise moment L_p, where a peak occurs (Fig. 3.3). It is important to note that the peaking property requires careful selection of an appropriate sequence $\mathbf{p}$. When the metric surpasses a given threshold λ_PD, a packet detection flag is raised. This same flag is also utilized as a timing reference.

From (3.4) it is straightforward to obtain an estimate of the CFO as

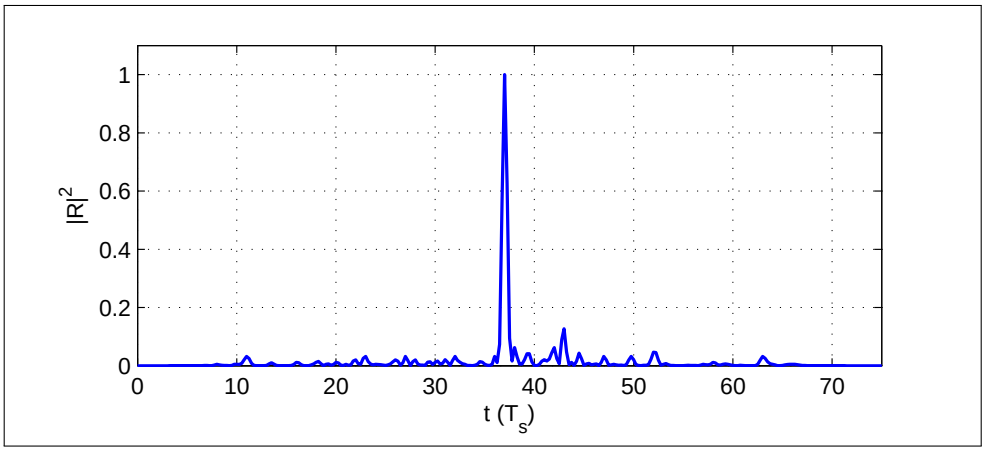

FIGURE 3.3. Normalized value of the correlation metric used for packet detection in the synchronization algorithm proposed by Feres (2013). If the peak is higher than a given threshold λ_{PD} a packet detection flag is raised. The peak also allows to identify the timing of the incoming packet.

$$\Delta\hat{f} = \frac{1}{2\pi T_{\mathrm{s}}} \angle \{R[L_{\mathrm{p}}]\} \quad , \tag{3.5}$$

where $\angle\{\cdot\}$ stands for the angle operation.

An analysis of the compatibility of the algorithm proposed by Feres (2013) with the scheme provided herein for setting up the SVD-BF is conducted in Chapter 5.

3.2.2 Automatic Gain Control

AGCs can be classified in two groups depending on whether the control loop is digital or analog. The advantages of a digital loop control are several. The primary advantage is the ease with which logical tests, based on short term changes of the signal levels and signal duration, can be implemented. Moreover, the responses to the logical tests can be more varied and larger in number than the available ones in a standard analog based control loop.

The AGC function can also be realized in two different ways according to the signal used for sensing the amplitude. If the VGA input signal is employed, the AGC loop moves forward in the receiver signal direction, so this loop is called ”feedforward loop”.

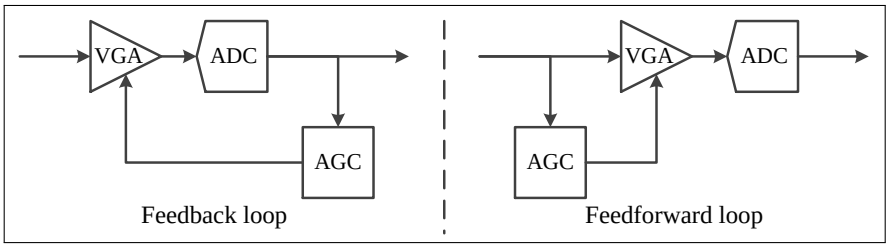

FIGURE 3.4. System structure of AGC.

By contrast, if the output VGA signal is sensed, the AGC is called a ”feedback loop”. Both structures are depicted in Fig. 3.4.

The main advantage of feedforward AGCs is the fast settling time. In contrast, the disadvantages are that the envelope detector is exposed to the entire dynamic range of the input signal and that the loop requires higher linearity. Particularly, some digital feedforward AGC have been proposed (Du, Jiang, Lin, & Sun, 2003; Vucic & Butorac, 2009), but they require high-resolution ADCs due to the large dynamic range of the signals. This is impractical for low-complexity solutions such as the LATINA UC testbed. For that reason, in this work, a feedback loop is proposed, which provides higher linearity and requires narrower dynamic range in the detector (Alegre, Celma, & Calvo, 2011). However, the challenge with this type of AGC is that the high level of feedback required to reach high VGA gain changes makes feedback loops more likely to exhibit instabilities if high input signal variations are observed. This type of loop will always have a maximum boundary bandwidth in order to maintain stability, which entails a minimum settling-time of the loop (Green, 1983).

Digital solutions where the VGA is also in the digital domain, like the proposed by Liang, Shi, Chen, and Xu (2010); Wen, Zhang, and Jiang (2011), are not suitable for low-complexity solutions, because they also need a large dynamic range.

Lee, Son, Choi, and Lee (2006) developed a very fast and stable digital AGC for a MIMO-OFDM WLAN receiver using a feedback scheme. Its fast response is achieved by a dual feedback loop. One does a coarse adjustment of the gain based on the saturation of the signal. The other feedback loop does a fine adjustment based on a comparison of the

power of the digital signal to a certain reference. Nevertheless, this design is for zero-IF receivers. This means it works with a complex baseband signal instead of an IF real signal, i.e. it operates with a signal of lower frequency and also requires more branches.

Jimenez, Fernandez-Getino Garcia, Serrano, and Armada (2004) presented a digital AGC that works with an IF signal. However, the algorithm assumes that a saturation flag given by the ADC is an indication that a packet has arrived, which can be used to determine when the AGC has to perform gain setting changes on the VGA. In applications like WSN using beamforming, where the main objective is to reach as far as possible with low-power consumption, this approach cannot be used. Most of the times the SNR of the signals at the receiver is low enough to not make the ADC to saturate. Hence, our AGC has to be designed to not require knowledge of the presence of a packet.

Perels, Burg, Haene, Felber, and Fichtner (2008) developed a completely digital feedback AGC for a MIMO-OFDM WLAN. It processes samples at digital IF of 20 MHz at a rate of 80 Msps. Nevertheless, this AGC comprises high-complexity computations, such as divisions, square-roots and logarithmic operations.

In this thesis, we propose a low-complexity design for a digital AGC and an analog VGA that uses a combination of the ideas previously presented. It is tested with an input IF signal of 6.75 Mhz, which is much noisier than its equivalent baseband signal. This test also considers the restrictive time needed to send the control signal from the digital signal processor to the VGA. The design and its corresponding results are provided in Chapter 5.

4. THE PING-PONG-PAYLOAD SCHEME

This chapter presents a low-complexity algorithm for setting up the strongest eigenchannel of the MIMO channel. Section 4.1 details the steps of the proposed scheme. The method for obtaining the vectors required for the beamforming is provided in Section 4.2. Finally, in Section 4.3 Monte Carlo simulations are conducted for studying the performance of the proposed scheme.

4.1 Proposed Scheme

The following MIMO scheme comprises a scenario where a source node *I* sends payload data to a destination node *II*, requiring of three stages (Fig. 4.1):

1. *Ping* transmission from node *I* to node *II* for channel training.
2. *Pong* transmission from node *II* to node *I* for channel-dependent reverse channel training.
3. *Payload* transmission from node *I* to node *II* with the actual payload data and an optional channel-dependent channel retraining.

Throughout this thesis, the proposed method is referred to as Ping-Pong-Payload (PPP) scheme. A block diagram of the PPP technique is shown in Fig. 4.2.

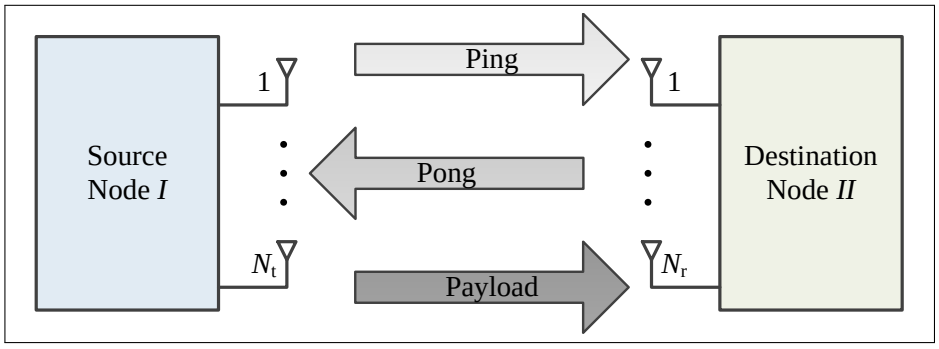

FIGURE 4.1. Representation of the Ping-Pong-Payload scheme between source node *I* and destination node *II*.

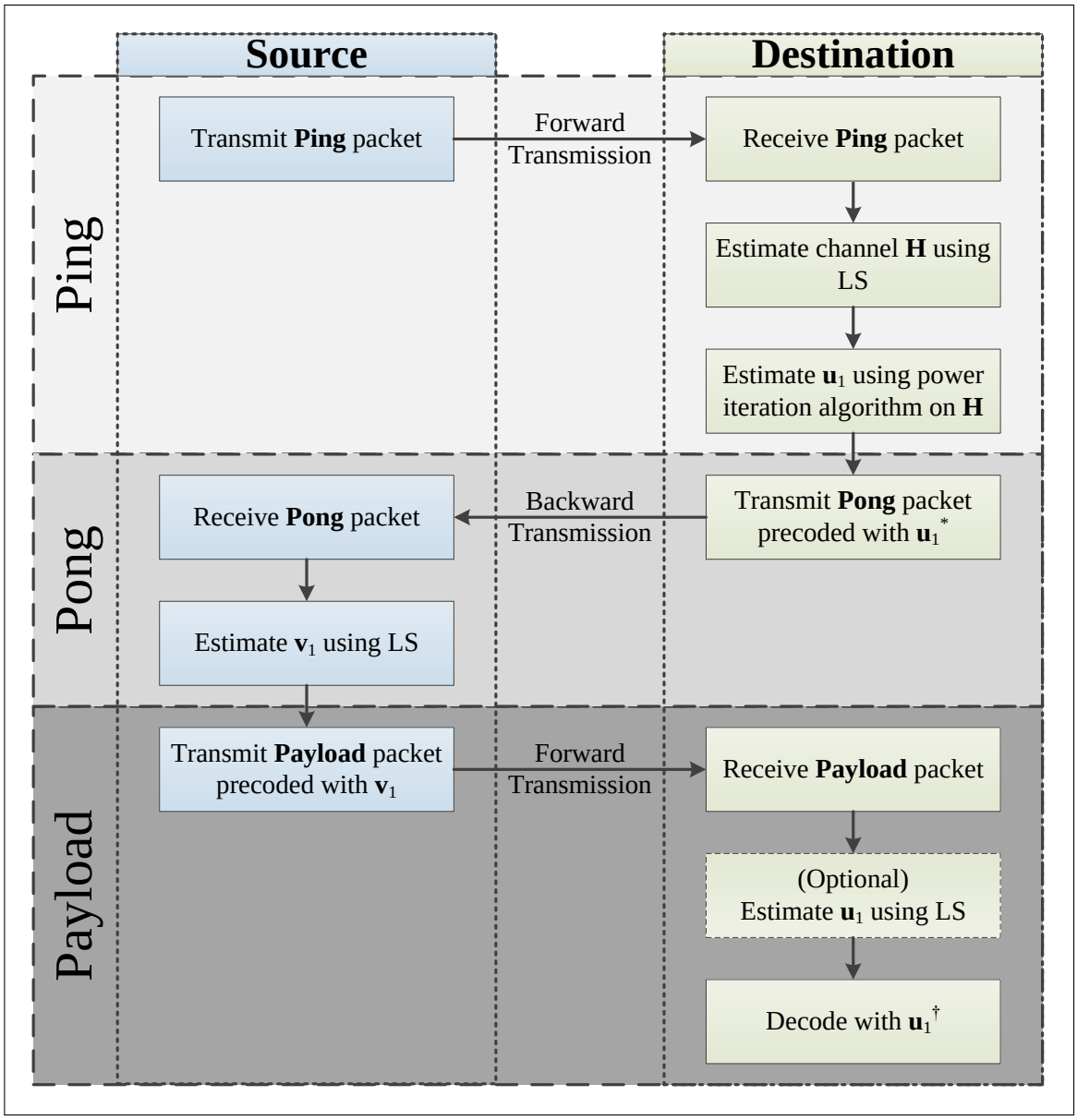

FIGURE 4.2. Summary of the Ping-Pong-Payload steps in each of the two nodes involved in the communication. The left side (blue) shows the steps of a node operating in a source mode. The right side (green), shows the steps of an identical node operating as a destination. The diagram is also divided in the three stages of the scheme: the Ping, Pong and Payload.

For the three stages of the PPP we assume a static channel, i.e. the mobility of the environment is slow enough to assume the coherence time is longer than the time required

for the three stages. We also assume channel reciprocity for forward and backward transmission between *I* and *II*.

4.1.1 Ping

The Ping consists of sending, from node *I* to node *II*, a known preamble sequence of symbols, represented by the column vector $\mathbf{a} \in \mathbb{C}^{L_\mathrm{a}}$, where L_a is the length of the Ping preamble. For computation efficiency at the receiver (Muñoz & Oberli, 2012), this sequence is sent in a staggered form such that $L_\mathrm{a}/N_\mathrm{t}$ training symbols are sent sequentially from each transmit branch as

$$\mathbf{X}_\mathrm{a} = \begin{bmatrix} a_1 & \cdots & a_{\frac{L_\mathrm{a}}{N_\mathrm{t}}} & 0 & \cdots & 0 & \cdots & 0 & \cdots & 0 \\ 0 & \cdots & 0 & a_{\frac{L_\mathrm{a}}{N_\mathrm{t}}+1} & \cdots & a_{\frac{2L_\mathrm{a}}{N_\mathrm{t}}} & & 0 & \cdots & 0 \\ \vdots & & \vdots & & & & \ddots & & & \\ 0 & \cdots & 0 & 0 & \cdots & 0 & & a_{\frac{(N_\mathrm{t}-1)L_\mathrm{a}}{N_\mathrm{t}}+1} & \cdots & a_{L_\mathrm{a}} \end{bmatrix} , \tag{4.1}$$

where each column represents a time slot and each row represents one antenna's transmissions over time. The element a_k corresponds to the k-th element of sequence $\mathbf{a}$.

The listened Ping is represented as

$$\mathbf{Y}_\mathrm{a} = \mathbf{H}\mathbf{X}_\mathrm{a} + \mathbf{N}_\mathrm{a} \ , \tag{4.2}$$

where $\mathbf{N}_\mathrm{a} \in \mathbb{C}^{N_\mathrm{r} \times L_\mathrm{a}}$ is the complex matrix of AWGN at receiver *II* during the Ping.

A least square (LS) estimation of the channel is performed at the destination node *II*. This minimum-variance unbiased estimator is used for not requiring channel and noise distributions knowledge. To use others estimators, such as the minimum mean square error (MMSE) estimator, the node would need to estimate the SNR. Additionally, the LS computation needs fewer operations (Muñoz & Oberli, 2012). The LS channel estimate at *II* is

$$\hat{\mathbf{H}} = \mathbf{Y}_{\mathrm{a}}\mathbf{X}_{\mathrm{a}}^{\dagger}\left(\mathbf{X}_{\mathrm{a}}\mathbf{X}_{\mathrm{a}}^{\dagger}\right)^{-1} \quad . \tag{4.3}$$

It should be noted that $\mathbf{X}_{\mathrm{a}}^{\dagger}\left(\mathbf{X}_{\mathrm{a}}\mathbf{X}_{\mathrm{a}}^{\dagger}\right)^{-1}$ can be precomputed and stored at the transceiver *II*, such that only one matrix multiplication is required.

Finally, the power iteration algorithm (PIA) explained in Section 4.2 is used to obtain an estimate $\hat{\mathbf{u}}_1$ of the first left singular from the matrix $\hat{\mathbf{H}}$.

4.1.2 Pong

Having the estimate $\hat{\mathbf{u}}_1$, device *II* transmits a training sequence of length L_{b} to device *I*. The training preamble is represented by the column vector $\mathbf{b} \in \mathbb{C}^{L_{\mathrm{b}}}$, where each element b_k of $\mathbf{b}$ corresponds to the k-th transmit symbol. The sequence is precoded as $\mathbf{X}_{\mathrm{b}} = \hat{\mathbf{u}}_1^{*}\mathbf{b}^{T}$, where $(\cdot)^{*}$ denotes the conjugate operator.

The communication of the Pong stage can be modeled as

$$\begin{aligned} \mathbf{Y}_{\mathrm{b}} &= \mathbf{H}^{T}\mathbf{X}_{\mathrm{b}} + \mathbf{N}_{\mathrm{b}} \\ &= \mathbf{V}^{*}\mathbf{\Sigma}^{T}\mathbf{U}^{T}\hat{\mathbf{u}}_1^{*}\mathbf{b}^{T} + \mathbf{N}_{\mathrm{b}} \quad , \end{aligned} \tag{4.4}$$

where $\mathbf{N}_{\mathrm{b}} \in \mathbb{C}^{N_{\mathrm{t}} \times L_{\mathrm{b}}}$ is the AWGN matrix at the receiver *I* during the Pong stage. By the SVD properties, we attain

$$\mathbf{Y}_{\mathrm{b}} \approx \sigma_1 \mathbf{v}_1^{*}\mathbf{b}^{T} + \mathbf{N}_{\mathrm{b}} \quad , \tag{4.5}$$

where the approximation sign stems from using an estimate $\hat{\mathbf{u}}_1$ instead of the actual $\mathbf{u}_1$. How good the approximation is depends on how good the estimate is.

An estimate of $\mathbf{v}_1$ can be obtained at the source *I* using LS as

$$\hat{\mathbf{v}}_1 = \frac{\left(\mathbf{Y}_{\mathrm{b}}\mathbf{b}^{*}\left(\mathbf{b}^{T}\mathbf{b}^{*}\right)^{-1}\right)^{*}}{||\mathbf{Y}_{\mathrm{b}}\mathbf{b}^{*}\left(\mathbf{b}^{T}\mathbf{b}^{*}\right)^{-1}||} \quad . \tag{4.6}$$

Again, the node *I* does not have to calculate $\mathbf{b}^* \left(\mathbf{b}^T \mathbf{b}^*\right)^{-1}$. Hence, the operation takes one matrix multiplication and one vector normalization.

4.1.3 Payload

Given that *I* has an estimate of the first right singular vector of the channel, it can precode and send the Payload packet with the data symbols to *II*. The data is represented by column vector $\mathbf{d} \in \mathbb{C}^{L_\mathrm{d}}$, which is precoded as $\mathbf{X}_\mathrm{d} = \hat{\mathbf{v}}_1 \mathbf{d}^T$. Node *II* thus receives

$$\mathbf{Y}_\mathrm{d} = \mathbf{H}\mathbf{X}_\mathrm{d} + \mathbf{N}_\mathrm{d} \ , \tag{4.7}$$

where $\mathbf{N}_\mathrm{d} \in \mathbb{C}^{N_\mathrm{r} \times L_\mathrm{d}}$ is the AWGN matrix in effect during the Payload stage.

The message is decoded such that $\tilde{\mathbf{y}}_\mathrm{d}^T = \hat{\mathbf{u}}_1^\dagger \mathbf{Y}_\mathrm{d}$, where vector $\tilde{\mathbf{y}}_\mathrm{d} \in \mathbb{C}^{L_\mathrm{d}}$ represents the decoded symbols and $\hat{\mathbf{u}}_1$ is the estimate calculated during the Ping. The equivalent received row vector corresponds to

$$\begin{aligned} \tilde{\mathbf{y}}_\mathrm{d}^T &= \hat{\mathbf{u}}_1^\dagger \mathbf{Y}_\mathrm{d} \\ &= \hat{\mathbf{u}}_1^\dagger \mathbf{H}\mathbf{X}_\mathrm{d} + \hat{\mathbf{u}}_1^\dagger \mathbf{N}_\mathrm{d} \\ &= \hat{\mathbf{u}}_1^\dagger \mathbf{U}\mathbf{\Sigma}\mathbf{V}^\dagger \hat{\mathbf{v}}_1 \mathbf{d}^T + \tilde{\mathbf{n}}_\mathrm{d}^T \\ &\approx \sigma_1 \mathbf{d}^T + \tilde{\mathbf{n}}_\mathrm{d}^T \ , \end{aligned} \tag{4.8}$$

where each noise element of $\tilde{\mathbf{n}}_\mathrm{d}^T = \hat{\mathbf{u}}_1^\dagger \mathbf{N}_\mathrm{d}$ has the same distribution of each element of $\mathbf{N}_\mathrm{d}$.

From (4.8) it can be noticed that for correct data detection, knowledge of σ_1 may be needed if the communication system uses amplitude modulation, such as quadrature amplitude modulation (QAM) or amplitude-shift keying amplitude (ASK). For obtaining σ_1, the following property can be used

$$\begin{aligned}\mathbf{u}_1^{\dagger}\mathbf{H}\mathbf{v}_1 &= \mathbf{u}_1^{\dagger}\mathbf{U}\boldsymbol{\Sigma}\mathbf{V}^{\dagger}\mathbf{v}_1 \\ &= \sigma_1 \ .\end{aligned} \tag{4.9}$$

Node *II* has knowledge of $\mathbf{u}_1$ and $\mathbf{H}$, both acquired during the Ping. Nonetheless, it lacks knowledge of $\mathbf{v}_1$. Hence, for using amplitude modulation, either feedback from node *I* or a computation over $\hat{\mathbf{H}}$ is necessary.

Intending to not increase the complexity of the scheme, we restrict the PPP to only utilize phase modulations, such as phase-shift keying (PSK). Furthermore, since it is more energy efficient to use small modulation sizes for long distance transmissions (Rosas & Oberli, 2012b), in this work we only use QPSK.

4.1.4 Payload with Beamforming Vector Re-estimation

Preambles are generally vital in every packet transmission for tasks such as packet detection, symbol timing and CFO correction. The preamble, can also be used to improve the performance of the PPP by re-estimating the vector $\mathbf{u}_1$ during Payload transmission as will be shown in Section 4.3. This new estimate has a smaller error than the one obtained at the Ping stage, because in the Payload transmission there is already an SNR gain, given by the beamforming precoding with $\hat{\mathbf{v}}_1$ at the transmitter. The improved scheme will be referred to as PPP with vector re-estimation (PPP-VR).

For re-estimating vector $\mathbf{u}_1$, node *I* also sends a Payload preamble $\mathbf{c} \in \mathbb{C}^{L_\mathrm{c}}$, being L_c its length, coded as $\mathbf{X}_\mathrm{c} = \hat{\mathbf{v}}_1\mathbf{c}^T$. The respective received signal is

$$\begin{aligned}\mathbf{Y}_\mathrm{c} &= \mathbf{H}\mathbf{X}_\mathrm{c} + \mathbf{N}_\mathrm{c} \\ &= \mathbf{U}\boldsymbol{\Sigma}\mathbf{V}^{\dagger}\hat{\mathbf{v}}_1\mathbf{c}^T + \mathbf{N}_\mathrm{c} \\ &\approx \sigma_1\mathbf{u}_1\mathbf{c}^T + \mathbf{N}_\mathrm{c} \ ,\end{aligned} \tag{4.10}$$

where $\mathbf{N}_{\mathrm{c}} \in \mathbb{C}^{N_{\mathrm{r}} \times L_{\mathrm{c}}}$ is the AWGN matrix in effect during the preamble symbols of the Payload stage.

Analogous to the Pong stage, an LS estimation can be optimally performed as it follows

$$\hat{\mathbf{u}}_1 = \frac{\mathbf{Y}_{\mathrm{c}}\mathbf{c}^* \left(\mathbf{c}^T\mathbf{c}^*\right)^{-1}}{||\mathbf{Y}_{\mathrm{c}}\mathbf{c}^* \left(\mathbf{c}^T\mathbf{c}^*\right)^{-1}||} \quad . \tag{4.11}$$

It is worth noting that there is no need to perform any algorithm to extract $\hat{\mathbf{u}}_1$ from $\hat{\mathbf{H}}$, as it was necessary for the Ping stage.

4.2 Singular Vector Computation

The computation of the first right singular vector is based on the PIA, which is explained in detail in Appendix A.

4.2.1 Power Iteration Algorithm

The PIA is originated from the following convergence property

$$\lim_{m\to\infty} \frac{\mathbf{W}^m\mathbf{z}_0}{||\mathbf{W}^m\mathbf{z}_0||} = \mathbf{u}_1 \quad , \tag{4.12}$$

where $\mathbf{W} = \mathbf{H}\mathbf{H}^{\dagger}$ and $\mathbf{z}_0 \in \mathbb{C}^{N_{\mathrm{r}}}$ is a random unit vector.

Since the destination node *II* has knowledge of $\mathbf{H}$, (4.12) could be used for computing $\mathbf{u}_1$. This idea suggests the need of a random number generator for $\mathbf{z}_0$. However, given the projection of $\mathbf{z}_0$ onto $\mathbf{u}_1$ is $\neq 0$ with probability 1 for any $\mathbf{z}_0$ (See Appendix A), the convergence of the algorithm does not depend on the actual election of $\mathbf{z}_0$, only its speed. Having a random $\mathbf{z}_0$ instead of a fixed vector gives no benefit if $\mathbf{u}_1$ is also random, which is the case. Without loss of generality we can reduce the computation complexity by choosing a fixed $\mathbf{z}_0$. Furthermore, by choosing a vector with only one non-zero element we reduce the number of sums and multiplications required, such as

$$\mathbf{z}_0 \triangleq \hat{\mathbf{e}}_1 = \begin{pmatrix} 1 \\ 0 \\ \vdots \\ 0 \end{pmatrix} . \tag{4.13}$$

Using the ideas already presented, the Algorithm 1 can be conducted for calculating $\hat{\mathbf{u}}_1$.

Algorithm 1 Power iteration algorithm

1: $\mathbf{W} \leftarrow \hat{\mathbf{H}}\hat{\mathbf{H}}^{\dagger}$
2: $\mathbf{z} \leftarrow \hat{\mathbf{e}}_1$
3: $n \leftarrow 1$
4: **while** $n < m$ **do**
5: $\quad \mathbf{z} \leftarrow \mathbf{W}\mathbf{z}$
6: $\quad n \leftarrow n + 1$
7: **end while**
8: $\hat{\mathbf{u}}_1 \leftarrow \frac{\mathbf{z}}{||\mathbf{z}||}$

TABLE 4.1. Operations for power iteration algorithm

Line	Sums	Products	Divisions	Square roots
1	$2N_{\mathrm{r}}^2\left(2N_{\mathrm{t}}-1\right)$	$4N_{\mathrm{t}}N_{\mathrm{r}}^2$	0	0
5	$2N_{\mathrm{r}}\left(2N_r-1\right)$	$4N_r^2$	0	0
8	$2N_{\mathrm{r}}-1$	$2N_{\mathrm{r}}$	N_{r}	1

The number of basic mathematical operations needed for each step of the algorithm can be found in Table 4.1, from where we can calculate the total cost $C_{\mathrm{PIA}}(m)$ of computing $\hat{\mathbf{u}}_1$ with m iterations as

$$C_{\text{PIA}}(m) = \begin{cases} N_{\text{r}}^2(4N_{\text{t}} + 4m - 2) - m & \text{sums} \\ 4N_{\text{t}}N_{\text{r}}^2 + 2mN_{\text{r}}(2N_{\text{r}} + 1) & \text{products} \\ N_{\text{r}} & \text{divisions} \\ 1 & \text{square roots} \end{cases} . \tag{4.14}$$

4.2.2 Reduced Power Iteration Algorithm

In the proposed PIA, there is a special case when $m = 1$. The result of the matrix multiplication of step 5 when $i = m = 1$ is

$$\begin{aligned} \mathbf{z}_1 &= \mathbf{W}\hat{\mathbf{z}}_0 \\ &= \hat{\mathbf{H}}\hat{\mathbf{H}}^{\dagger}\hat{\mathbf{e}}_1 \\ &= \hat{\mathbf{H}}\hat{\mathbf{H}}^{\dagger}_{1,1:N_{\text{t}}} \ , \end{aligned} \tag{4.15}$$

where $\hat{\mathbf{H}}_{1,1:N_{\text{t}}}$ denotes the first row of $\hat{\mathbf{H}}$. Noting that $\mathbf{W}$ is not needed, we can use the Algorithm 2 as a reduced version of Algorithm 1 to obtain $\hat{\mathbf{u}}_1$.

Algorithm 2 Reduced power iteration algorithm

1: $\mathbf{z} \leftarrow \hat{\mathbf{H}}\hat{\mathbf{H}}^{\dagger}_{1,1:N_{\text{t}}}$
2: $\hat{\mathbf{u}}_1 \leftarrow \frac{\mathbf{z}}{||\mathbf{z}||}$

TABLE 4.2. Operations for reduced power iteration algorithm

Line	Sums	Products	Divisions	Square roots
1	$2N_{\text{r}}\,(2N_{\text{t}} - 1)$	$4N_{\text{t}}N_{\text{r}}$	0	0
2	$2N_{\text{r}} - 1$	$2N_{\text{r}}$	N_{r}	1

The total cost of the reduced power iteration algorithm (RPIA) can be inferred from Table 4.2 as

$$C_{\text{RPIA}} = \begin{cases} 4N_{\text{r}}N_{\text{t}} - 1 & \text{sums} \\ 4N_{\text{t}}N_{\text{r}} + 2N_{\text{r}} & \text{products} \\ N_{\text{r}} & \text{divisions} \\ 1 & \text{square roots} \end{cases} . \tag{4.16}$$

4.2.3 Computational Cost Comparison

To study the computation complexity of the PIA, the GRA is used as a reference. GRA consists of two phases: A bidiagonalization and a superdiagonal reduction. The first phase turns an arbitrary complex matrix into a bidiagonal matrix, which is a matrix with all entries equal to zero except the diagonal and superdiagonal. The second phase of the GRA reduces the upper diagonal terms into zero. This last process phase is constituted by a series of Givens rotations, which make the matrices to converge toward zero (Golub & Van Loan, 1996).

In Rosas (2012) a study of the computation cost of the GRA is conducted. This study states that the total cost of performing the SVD for an $N \times N$ matrix is

$$C_{\text{GRA}} = \begin{cases} \frac{16}{3}N^3 + 10N^2 - \frac{28}{3}N + 10 & \text{sums} \\ \frac{16}{3}N^3 + 16N^2 - \frac{70}{3}N + 4 & \text{products} \\ 4N^2 - 2N - 3 & \text{divisions} \\ 2N^2 - 3 & \text{square roots} \\ 2N - 3 & \text{sign operations} \end{cases} . \tag{4.17}$$

Using the parameters of Rosas and Oberli (in press), we can calculate the number of cycles an Arithmetic Logic Unit (ALU) requires to perform the decomposition using the different methods. The results are shown in Fig 4.3. As can be seen, the lowest complexity is achieved by the RPIA, which in the case of a MIMO channel of 16×16 is less than 4% of the GRA.

When comparing the computation complexity in terms of ALU cycles per element obtained, the GRA requires fewer operations than the PIA (Fig 4.4). Nevertheless, the

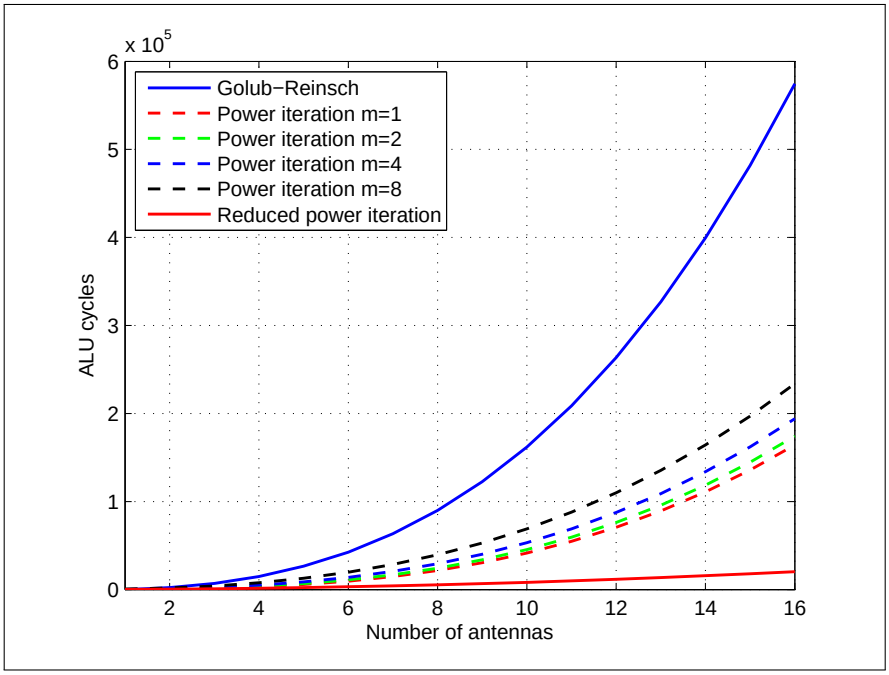

FIGURE 4.3. ALU cycles needed to perform the Golub-Reinsch, the power iteration and the reduced power iteration algorithms for different antenna array sizes.

RPIA still requires fewer operations than the GRA, because the GRA, contrary to the RPIA, does not allow computing only the first singular vector, it demands computing the entire SVD.

4.3 Simulation Results

In this section, the performance of the PPP scheme is evaluated with computer simulations. The elements of the channel matrix $\mathbf{H}$ are generated randomly for each run as i.i.d. circularly symmetrical complex Gaussian random variables with zero mean and unit variance. In addition, we generate the noise samples randomly as i.i.d. circularly symmetrical complex Gaussian random variables with zero mean and variance ν^2. The simulations were performed in a MIMO configuration of 4×4.

The preambles are composed by $L = 32$ symbols (i.e. $L = L_{\mathrm{a}} = L_{\mathrm{b}} = 32$) and a Payload packet of 1000 bits of information.

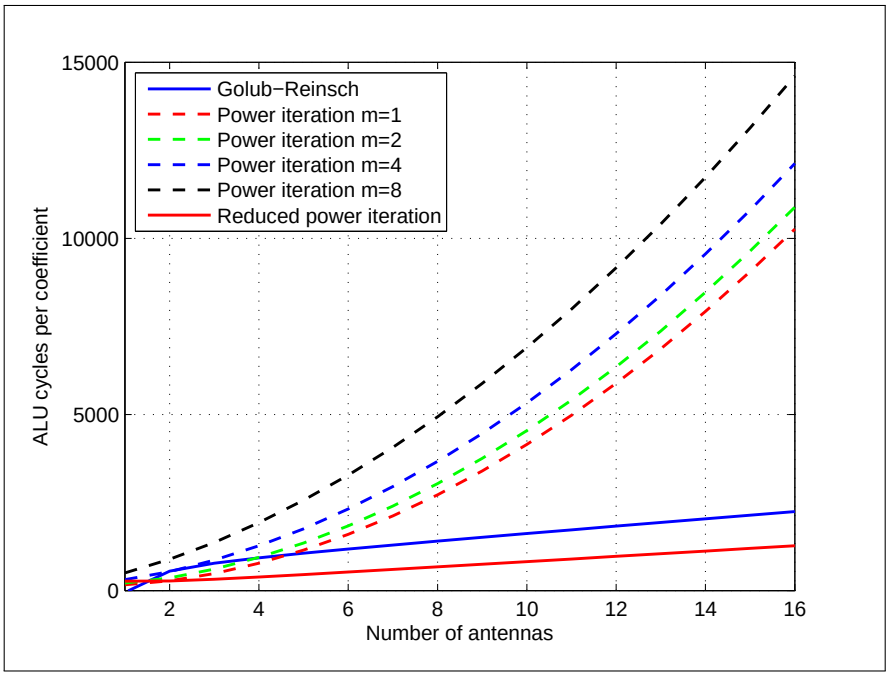

FIGURE 4.4. ALU cycles per coefficient needed to perform the Golub-Reinsch, the power iteration and the reduced power iteration algorithms for different antenna array sizes.

We compare the PPP with the base case (i.e. SISO) and MRC, which is the optimal for SIMO systems. To make a fair analysis, we considered the same total symbols for channel training and the same total transmitted preamble energy. Fig. 4.5 shows the resulting BER of PPP without re-estimation and the others schemes. As can be seen, PPP outperforms MRC, even when $m = 1$ iterations (red dashed line) are conducted. With $m = 10$ (black dashed line) the results are equivalent to an SNR loss of less than 0.1 dB with respect to the results that could be achieved with the same channel estimate using a perfect SVD. Finally, the difference in BER between the PPP with the highest number of iterations, i.e. $m = 10$, and the theoretical SVD-BF (magenta solid line) is explained by the errors produced at the channel estimation.

To study the impact of channel estimation on the performance of the PPP without re-estimation, simulations with preambles of length $L = 4$, $L = 32$ and $L = 128$ symbols are compared in Fig. 4.6. As intuition suggests, as the preamble grows in length, the

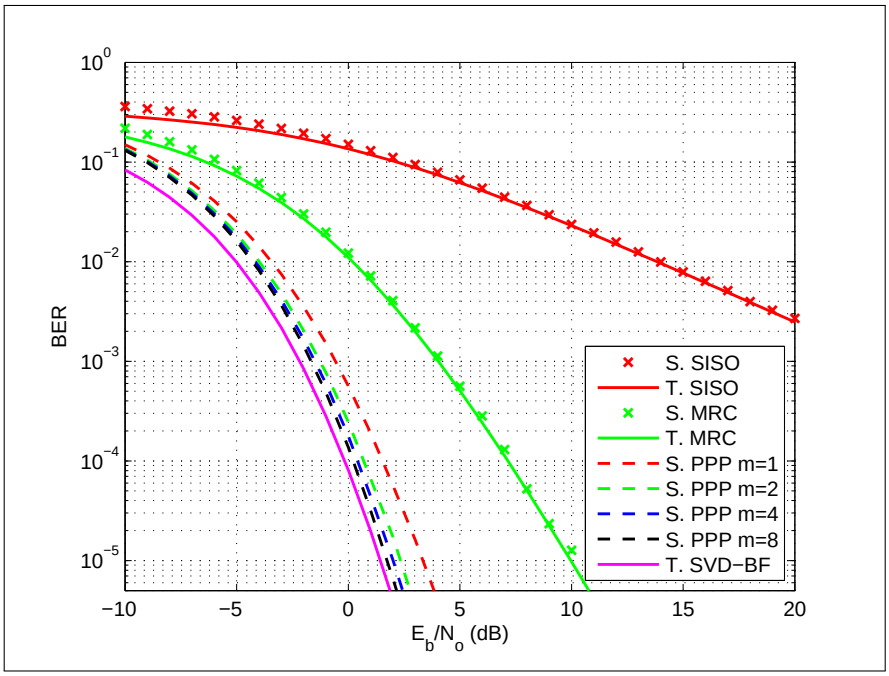

FIGURE 4.5. BER over a 4×4 MIMO channel with SISO, MRC and PPP schemes. S stands for simulated and T for theoretical.

BER approaches the theoretical curve of SVD-BF. Despite the diminishing returns of the preamble growth, the impact of the number of iterations of the PIA is almost constant.

The same simulations were carried out implementing the re-estimation of vector $\mathbf{u}_1$ at the Payload stage. The corresponding BER comparison with the basic PPP scheme can be seen in Fig. 4.7. The results suggest that performing an extra iteration is almost equivalent to re-estimate the vector at the Payload. In the case when $m = 1$, the SNR gain given by the re-estimation can be as high as 1 dB.

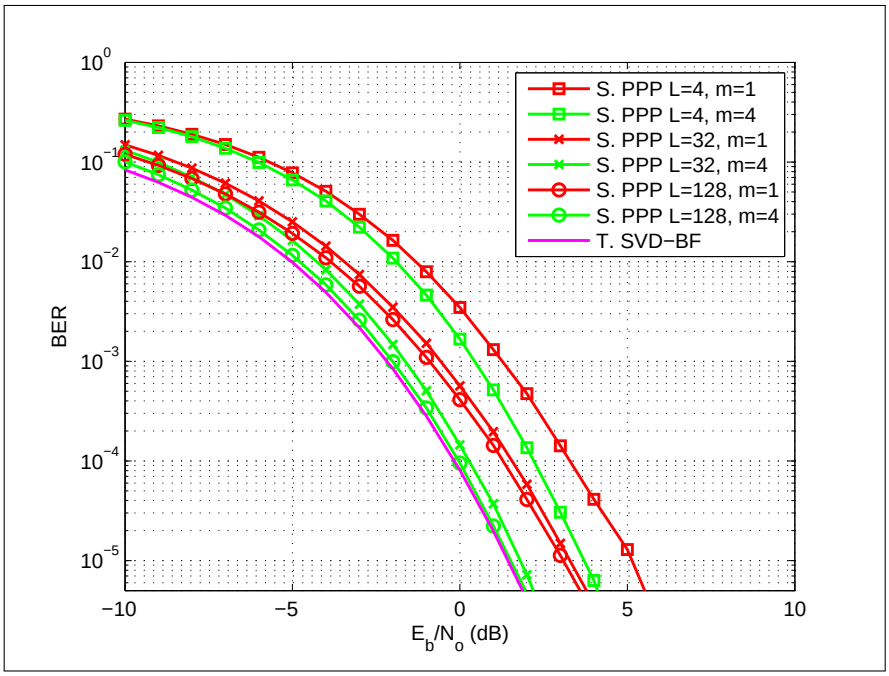

FIGURE 4.6. BER comparison with $L = 4$, $L = 32$ and $L = 128$ symbols for channel training, and $m = 1$ and $m = 5$ iterations of the PIA. S stands for simulated and T for theoretical.

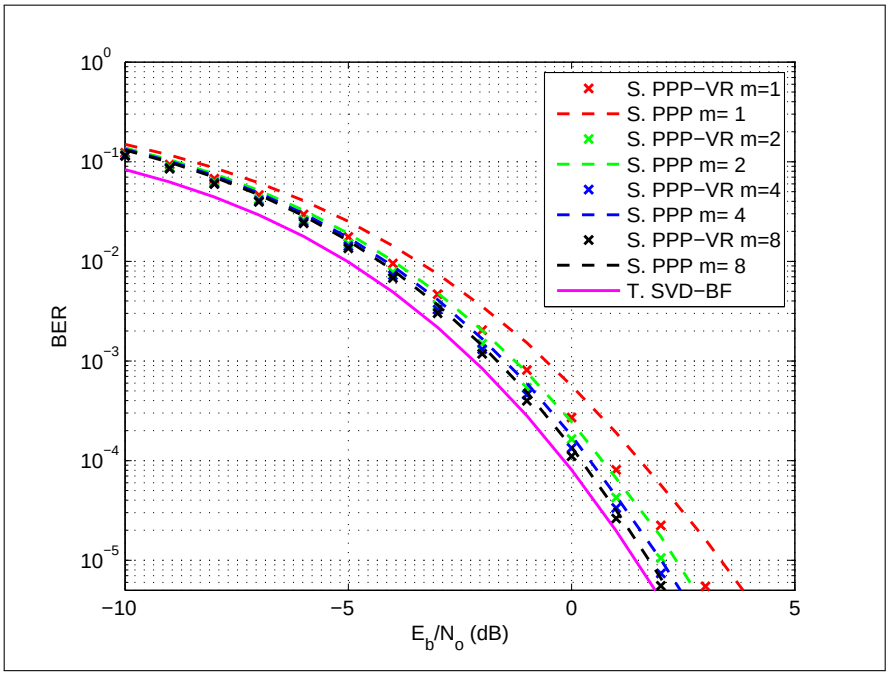

FIGURE 4.7. BER comparison with and without beamforming vector re-estimation at Payload stage. S stands for simulated and T for theoretical.

5. IMPLEMENTATION CONSIDERATIONS

The main goal in Chapter 4 was to reach a BER close to the theoretical SVD-based beamforming. In fact, the result is a low-complexity technique that takes advantages of channel reciprocity for reducing the overhead and computes only one beamforming vector instead of the full SVD. In order to implement this scheme, an study of the acquisition of each of the transmitted packets must be conducted. The acquisition comprises the synchronization of the receiver and the channel estimation. Moreover, for testing the proposed scheme in the LATINA UC testbed, an appropriate AGC is designed. Finally, these considerations are utilized for simulating the PPP with the testbed specifications.

5.1 Ping-Pong-Payload Acquisition

5.1.1 Synchronization

The three stages of the PPP have to perform the synchronization tasks. Otherwise, they would lack the correct timing and CFO correction needed to perform the channel estimation and data detection.

Since the symbol sequences $\mathbf{a}$, $\mathbf{b}$ and $\mathbf{c}$ (optional), used for channel training in the Ping, Pong and Payload, respectively (Section 4.1), correspond to any QPSK symbols, they can be set according to the sequences proposed by Feres (2013). This allows for employing the same sequences for synchronization and channel estimation. The joint use of the preamble helps to reduce the overhead and thereafter the energy spent in the transmission.

For the Ping stage, no modification of the synchronization algorithm proposed by Feres (2013) is required, since both techniques need to send the sequence in an staggered configuration along the transmit antennas. Conversely, as it was described in Chapter 4, the training sequences for the Pong and Payload stage cannot be sent in a staggered form and have to be weighted on the different antennas according to the singular vectors. However, the correlation of the synchronization algorithm can still be performed as displayed below.

In the case of the Pong, (3.4) is modified

$$\begin{aligned} R[L_{\mathrm{p}}] &= \frac{E_s}{N_{\mathrm{r}}} e^{j2\pi\Delta f T_{\mathrm{s}}} \sum_{i=1}^{N_{\mathrm{r}}} \left|\sigma_1 v_{i,1}^*\right|^2 + n_{\mathrm{R}}[L_{\mathrm{p}}] \\ &= \frac{E_s \sigma_1^2}{N_{\mathrm{r}}} e^{j2\pi\Delta f T_{\mathrm{s}}} + n_{\mathrm{R}}[L_{\mathrm{p}}] \ , \end{aligned} \tag{5.1}$$

where $v_{i,1}$ is the i-th element of vector $\mathbf{v}_1$. Analogous, the Payload correlation at the exact moment $k = L_{\mathrm{p}}$ corresponds to

$$\begin{aligned} R[L_{\mathrm{p}}] &= \frac{E_s}{N_{\mathrm{r}}} e^{j2\pi\Delta f T_{\mathrm{s}}} \sum_{i=1}^{N_{\mathrm{r}}} \left|\sigma_1 u_{i,1}\right|^2 + n_{\mathrm{R}}[L_{\mathrm{p}}] \\ &= \frac{E_s \sigma_1^2}{N_{\mathrm{r}}} e^{j2\pi\Delta f T_{\mathrm{s}}} + n_{\mathrm{R}}[L_{\mathrm{p}}] \ , \end{aligned} \tag{5.2}$$

being $u_{i,1}$ the i-th element of vector $\mathbf{u}_1$.

As it is evident, both the metric for packet detection and the estimate of the CFO remain exactly the same, except for gain constants.

5.1.2 Channel Estimation

Channel estimation plays a key role in the performance of the system. Its quality depends on the length of the training preamble, the SNR at which it is obtained and the number of transmit branches (N_{t}). Fig. 5.1 shows the SNR loss of BER curves in a system using SVD-BF due to the effect of the preamble length and the SNR. Intuitively, the longer the preamble, the better the channel estimation and as a result the lower the BER. Conversely, as SNR increases, the channel estimation also improves making the BER to approach the theoretical one (with perfect CSI).

a) Distortion due to AGC

In 5.1.1 the idea of using the same preamble for both synchronization and channel training was proposed. However, in a system where the training sequence is orthogonal

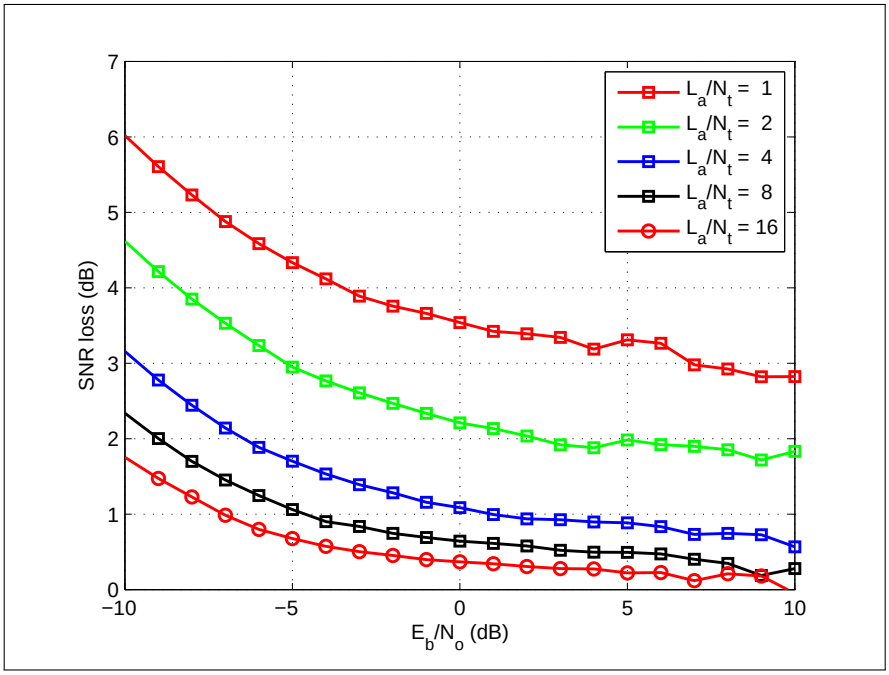

FIGURE 5.1. Perfomance loss in 2×2 SVD-BF due to imperfect CSI considering different training preamble lengths.

in time (staggered preamble), as it is the case, the AGC has an impact on the channel estimation and thereafter on the performance of the system.

As it was described in Section 2.2, an AGC adjusts the gain of a VGA so that the dynamic range of the ADC is used optimally, i.e. not saturating the ADC and keeping the quantization noise negligible compared to thermal noise. During idle reception, the AGC runs essentially freely adjusting the power of the incoming analog signal in order to ensure that the ADC output is useful for digital packet detection. Once a packet is detected, the gain of the VGA can be locked for the remaining of the message. Therefore, the VGA gain usually changes during channel estimation, which has an impact on the quality of the estimates. Most of the industry MIMO standards (e.g. IEEE 802.11n, WiMAX, LTE) utilize one preamble for AGC stabilization and packet detection and another one for channel estimation. Hence, the gains of the VGAs are already locked when the channel estimation is performed.

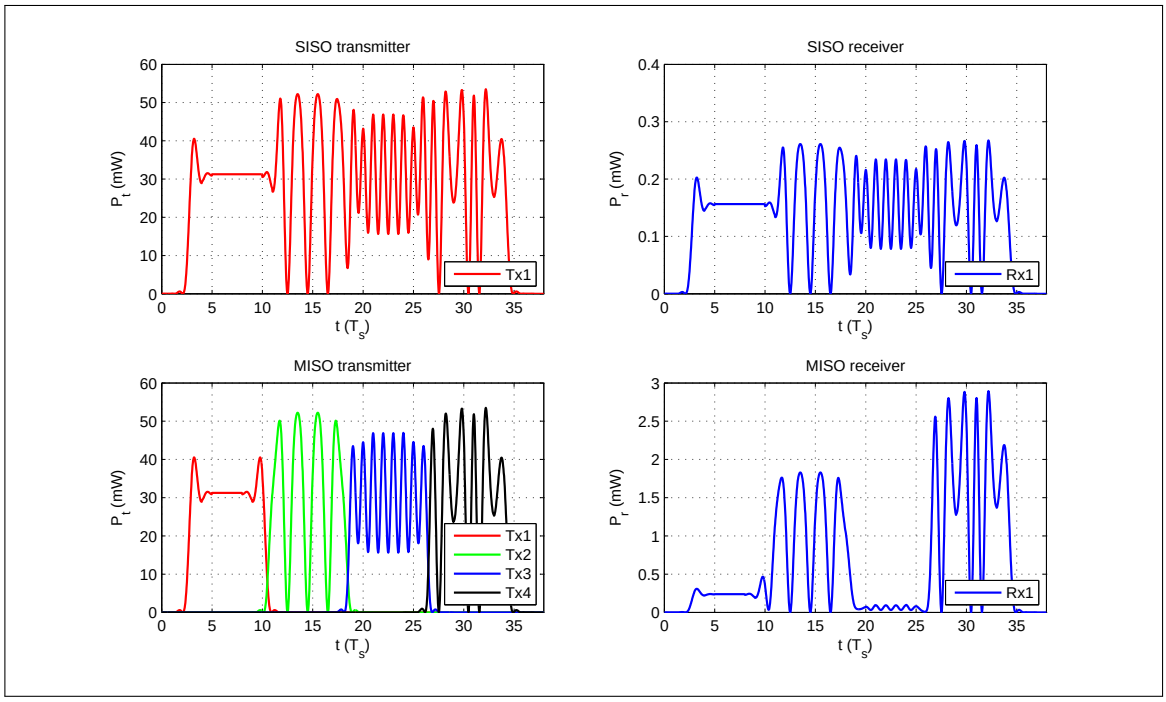

FIGURE 5.2. Representation of the received power compared to the transmitted one in SISO (top) and MISO (bottom). In the SISO case the transmitted signal (top left) and the respective received signal (top right) have constant average power. In the MISO case, the signal is sent from different antennas with a constant average power but only one transmitting at the same time (bottom left). The respective received signal (bottom right) changes its average power according to the different path gains between the transmit antennas and the receive one.

In a SISO communication, if the channel is static, the average power of the received signal is constant throughout the transmission. Hence, the VGA gain required does not change much. By contrast, in a MISO or MIMO communication, in which only one antenna j transmits at any time and the transmitted power is constant over the entire packet (e.g. Ping preamble), the received signal power will vary according to the respective channel realization $h_{i,j}$ between transmit antenna j and receive antenna i. This means that each sub-sequence transmitted by a single antenna needs a different VGA gain associated in the receiver. In order to illustrate the point, Fig. 5.2 shows the SISO case on the top and the MISO case on the bottom.

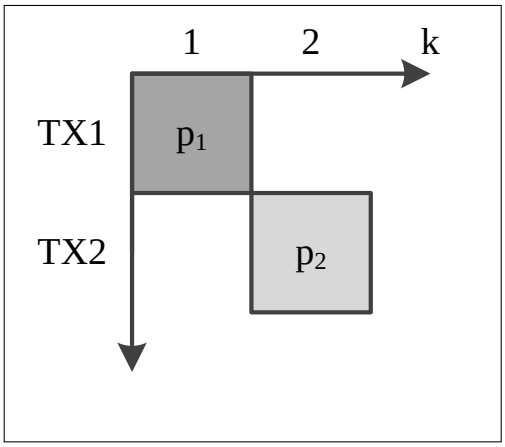

FIGURE 5.3. Staggered 2×2 MIMO preamble where each block represents a training symbol.

The situation may be modeled mathematically as follows. For simplicity we consider a 2×2 MIMO system

$$\begin{aligned} \mathbf{y}[k] &= \mathbf{H}\mathbf{x}[k] + \mathbf{n}[k] \\ \begin{pmatrix} y_1[k] \\ y_2[k] \end{pmatrix} &= \begin{bmatrix} h_{1,1} & h_{1,2} \\ h_{2,1} & h_{2,2} \end{bmatrix} \begin{pmatrix} x_1[k] \\ x_2[k] \end{pmatrix} + \begin{pmatrix} n_1[k] \\ n_2[k] \end{pmatrix} \quad , \end{aligned} \tag{5.3}$$

where $y_i[k]$ is the k-th symbol received at antenna i, before the AGC.

A simplified model of the AGC considers a digital symbol $\breve{y}_i[k] = q_i[k]y_i[k]$, where $q_i[k]$ is the VGA gain at the antenna i at the discrete time k such that the average power over each subsequence is maintained almost constant throughout the transmission. In order to accomplish that, a power reference P_{ref} is utilized.

Considering a staggered preamble of one symbol per transmit antenna, as it is depicted in Fig. 5.3, the received signal at $k = 1$ is

$$\begin{aligned}\begin{pmatrix}\check{y}_1[1]\\ \check{y}_2[1]\end{pmatrix} &= \begin{bmatrix}q_1[1] & 0\\ 0 & q_2[1]\end{bmatrix}\left(\begin{bmatrix}h_{1,1} & h_{1,2}\\ h_{2,1} & h_{2,2}\end{bmatrix}\begin{pmatrix}p_1\\ 0\end{pmatrix} + \begin{pmatrix}n_1[1]\\ n_2[1]\end{pmatrix}\right)\\ &= \begin{pmatrix}q_1[1]\left(h_{1,1}p_1 + n_1[1]\right)\\ q_2[1]\left(h_{2,1}p_1 + n_2[1]\right)\end{pmatrix}\quad ,\end{aligned} \tag{5.4}$$

and for $k = 2$ is

$$\begin{aligned}\begin{pmatrix}\check{y}_1[2]\\ \check{y}_2[2]\end{pmatrix} &= \begin{bmatrix}q_1[2] & 0\\ 0 & q_2[2]\end{bmatrix}\left(\begin{bmatrix}h_{1,1} & h_{1,2}\\ h_{2,1} & h_{2,2}\end{bmatrix}\begin{pmatrix}0\\ p_2\end{pmatrix} + \begin{pmatrix}n_1[2]\\ n_2[2]\end{pmatrix}\right)\\ &= \begin{pmatrix}q_1[2]\left(h_{1,2}p_2 + n_1[2]\right)\\ q_2[2]\left(h_{2,2}p_2 + n_2[2]\right)\end{pmatrix}\quad .\end{aligned} \tag{5.5}$$

With the received signals we can attain the corresponding LS channel estimate as

$$\hat{\mathbf{H}} = \begin{bmatrix}q_1[1]\left(h_{1,1} + \tilde{n}_1[1]\right) & q_1[2]\left(h_{1,2} + \tilde{n}_2[1]\right)\\ q_2[1]\left(h_{2,1} + \tilde{n}_1[2]\right) & q_2[2]\left(h_{2,2} + \tilde{n}_2[2]\right)\end{bmatrix}\quad , \tag{5.6}$$

where $\tilde{n}_i[k] = n_i[k]p_k$. We can notice that the estimate $\hat{\mathbf{H}}$ is distorted from the original channel $\mathbf{H}$ not only by the effect of the noise, but also by the effect of the VGA gains. Fig. 5.4 shows the loss of performance in SVD-BF when the AGC gain distortion is present in the channel estimate. In low SNR scenarios the performance improves as the SNR increases, because the gain of the AGC is dominated by the effect of the thermal noise, whose power is relatively constant and independent of the transmit antenna. Conversely, at high SNR, the performance deteriorates with an increase of the SNR, as the AGC is dominated by the effect of the channel realizations, which are different for each transmit antenna. As an illustration of this, Fig. 5.5 depicts the ratio between the largest and smallest VGA gain, i.e. $\frac{\max q_i[j]}{\min q_i[j]}$.

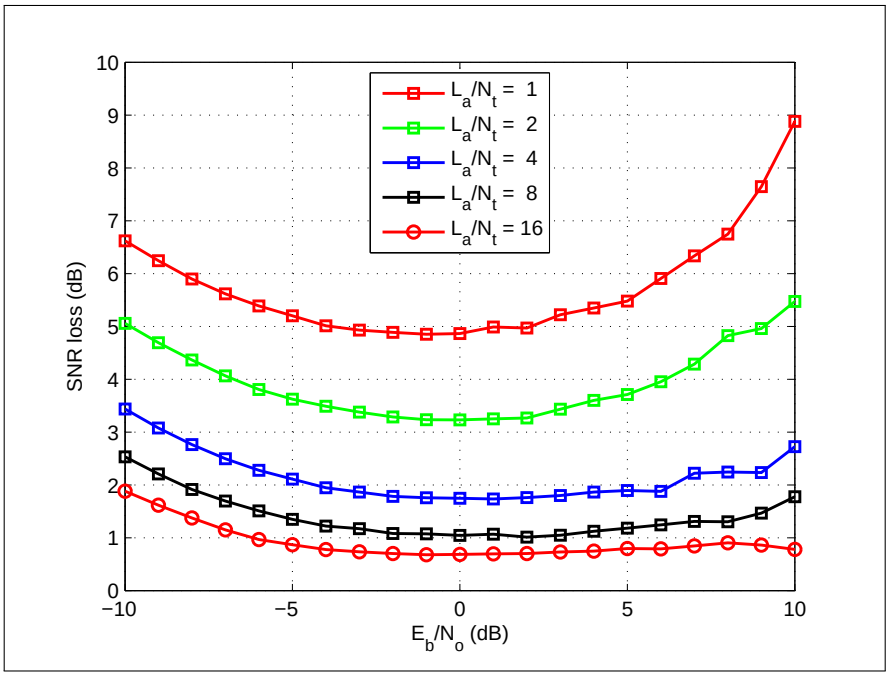

FIGURE 5.4. Perfomance loss in 2×2 SVD-BF due to imperfect CSI with AGC gain distortions for different training preamble lengths.

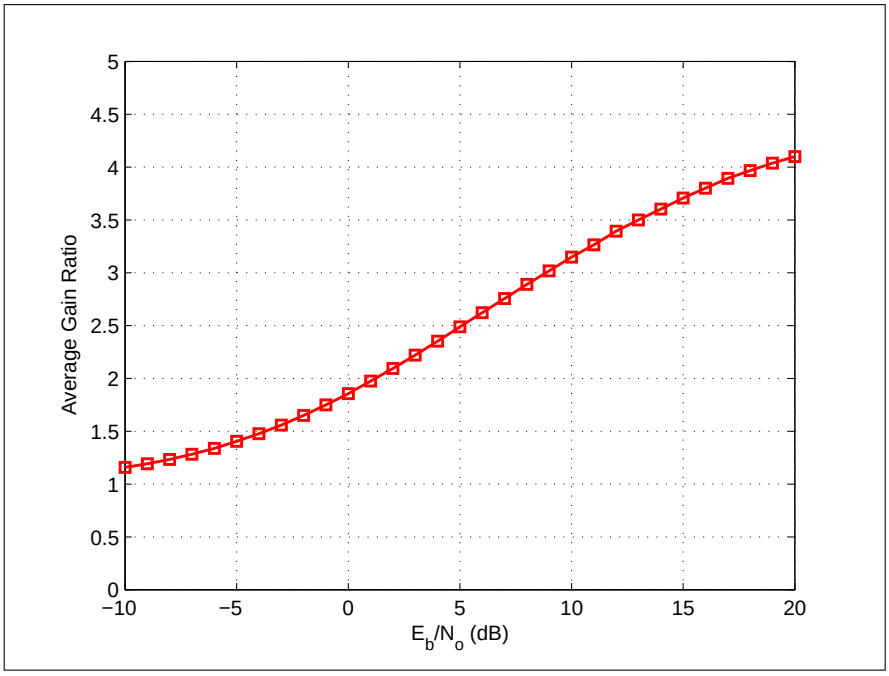

FIGURE 5.5. Average $\frac{\max q_i[j]}{\min q_i[j]}$. As the SNR increases, the effect of the noise becomes less important, which increases the effect of different channel realizations. Hence, the ratio of the gains increases.

b) Wideband Noise Effect

When a receiver listens for a signal, it only does it in a reduced portion of the spectrum. In order to do that, a band-pass filter (BPF), centered on the carrier frequency f_c and with the same bandwidth B_{I} of the incoming signal, should be used. Nonetheless, it is difficult to design analog narrow BPF with a relative high center frequency. To solve that, the same is done at the IF. However, the bandwidth of this filter can never be the same as the signal bandwidth B_{I}. Therefore, the receiver's front end works with a bandwidth $B_{\text{W}} > B_{\text{I}}$. Recalling that the noise power is given by $N_0 B$, the noise that reaches the ADC has higher power than the in-band noise. Only downstream, in the digital baseband processing, this extra noise can be removed due to the ease of developing an appropriate digital LPF. Fig. 5.6 represents the spectrum of both the in-band and wideband cases.

We can understand the implications of the wideband noise by modifying (5.3) as

$$\mathbf{y}_{\text{W}}[k] = \mathbf{H}\mathbf{x}[k] + \mathbf{n}_{\text{W}}[k] \ , \tag{5.7}$$

where $\mathbf{y}_{\text{W}}[k]$ is the received wideband vector at sample k and $\mathbf{n}_{\text{W}}[k]$ is the respective wideband noise vector with power $N_0 B_{\text{W}}$. The relationship between the in-band and wideband model is

$$\begin{aligned} \text{LPF}\{\mathbf{y}_{\text{W}}[k]\} &= \text{LPF}\{\mathbf{H}\mathbf{x}[k] + \mathbf{n}_{\text{W}}[k]\} \\ &= \mathbf{H}\mathbf{x}[k] + \mathbf{n}[k] \\ &= \mathbf{y}[k] \ , \end{aligned} \tag{5.8}$$

where LPF$\{\cdot\}$ means a low-pass filtering with bandwidth B_{I}.

In Fig. 5.7 can be seen that the higher the ratio between the B_{W} and B_{I}, the smaller the SNR loss due to AGC gain distortions. This does not consider that using a larger bandwidth at the front end reduces the resolution of the ADC. Hence, supposing that the ADC resolution is not a limitation, the fact that the power of the noise is higher at the ADC

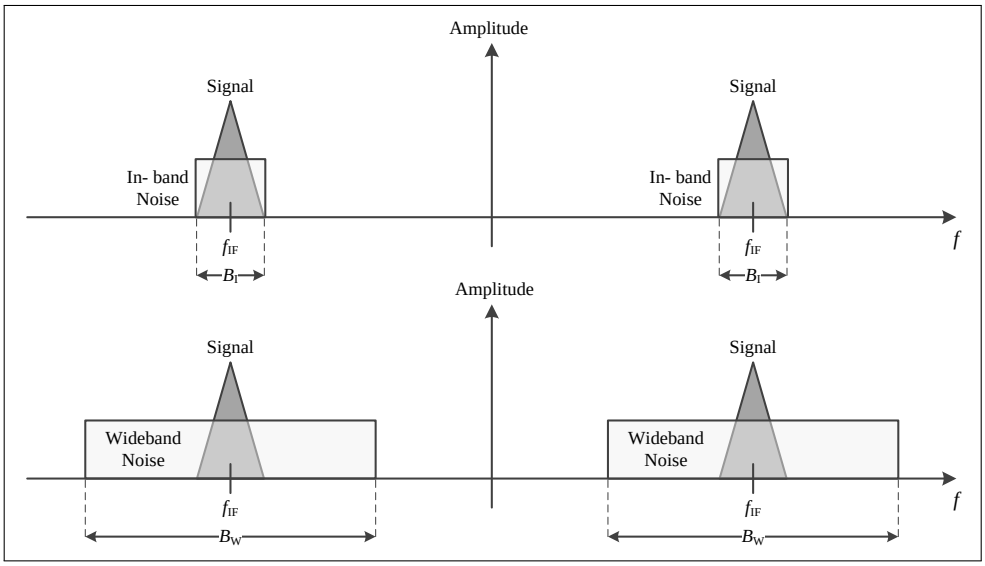

FIGURE 5.6. Frequency spectrum representation of the signal with both in-band (top) and wideband (bottom) noise.

output helps to reduce the impact of the effect of the channel realizations by reducing the variability of the VGA gains.

c) Solution

One way of reversing the distortion is to divide each element of $\hat{\mathbf{H}}$ in (5.6) by the corresponding $q_i[k]$. This is impractical for two reasons:

1. A digital division is a complex operation when it is not by a power of 2. Hence, a low-complexity transceiver design should avoid them if possible.
2. Given the gains of the VGA are floating before the packet detection, a register of the same length of the preamble is needed for storing the corresponding gains, which may increase the size of the transceiver.

In the Section 5.3 we evaluate the loss of performance of the PPP due the distortions the AGC introduces in the channel estimate. This evaluation is performed in the LATINA UC testbed simulator, which includes a real-time digital AGC.

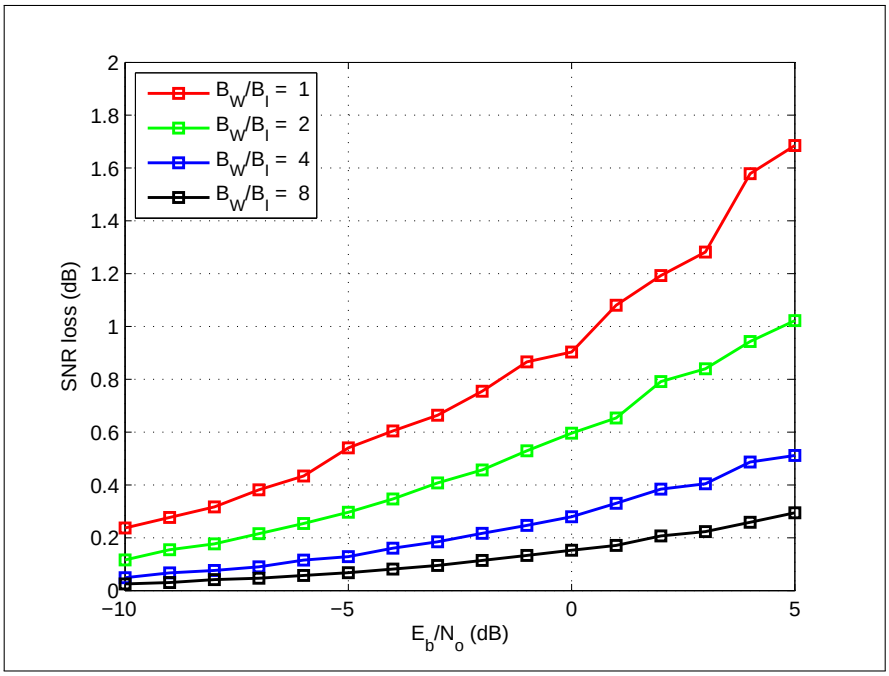

FIGURE 5.7. Perfomance loss in 2×2 SVD-BF due to imperfect CSI with AGC gain distortions for different wideband/in-band noise ratios.

5.2 Automatic Gain Control

5.2.1 Digital Design

We define $r_{\text{IF}}(t)$ as the received signal before the VGA, such that

$$r_{\text{IF}}(t) = \Re\left\{\sqrt{2}\left(\sqrt{E_{\text{s}}}hs_{\text{BB}}(t) + n_{\text{BB}}(t)\right)e^{j2\pi f_{\text{IF}}t}\right\} \quad , \tag{5.9}$$

where f_{IF} corresponds to the IF frequency. We also define the signal at the VGA output as

$$r_{\text{v}}(t) = q(t)r_{\text{IF}}(t) \tag{5.10}$$

where $q(t) > 0$ is the VGA gain over the received IF signal.

$r_{\mathrm{v}}(t)$ is sampled at a rate $\frac{N_{\mathrm{up}}}{T_{\mathrm{s}}}$ and quantized in N_{b} bits, by the ADC. We define $r_{\mathrm{d}}[k]$ as the k-th digital sample of $r_{\mathrm{v}}(t)$. Hence, $r_{\mathrm{d}}[k] = r_{\mathrm{v}}\left(k\frac{N_{\mathrm{up}}}{T_{\mathrm{s}}}\right)$.

The proposed AGC consists of a dual feedback loop: one for coarse action, which decreases dramatically the gain when there is an abrupt rise in the energy (i.e. when a packet begins to arrive); and the other one for fine action, which adjusts the gain based on an energy comparison. It is to note that no coarse gain increase is necessary, because this would be needed when the receivers stops listening for a packet, and this adjustment can be done with a slow fine adjustment.

The coarse action loop consists of the upper branch depicted in Fig. 5.8. A saturation detector indicates at every sample k if $r_{\mathrm{d}}[k]$ has reached the upper or lower limit of the ADC, i.e. if $r_{\mathrm{d}}[k] = 2^{N_{\mathrm{b}}-1} - 1$ or $r_d[k] = -2^{N_{\mathrm{b}}-1}$, where $2^{N_{\mathrm{b}}}$ are all the possible integer values. An accumulator is used such that when its value surpasses a threshold λ_{sat} a coarse action flag is raised. The accumulator is reset to zero every time there is no saturation flag. Hence, a coarse action is performed only when λ_{sat} consecutive samples of the incoming signal are saturated.

The other branch implements a square-law detector, which is commonly used in AGC systems. They exhibit an instantaneous output that is proportional to the square of the IF input voltage. Thus, the output is directly proportional to the input power. When used with a wideband AGC loop, the square-law detector provides an average output independent of the modulation. Just as in the case of a simple envelope detector, the rectified output can only be positively affected by the LPF incorporated into the loop. This results in the loop having a limited instantaneous response to fast transitions in the IF signal amplitude (Drentea, 2010). The LPF of the signal power $P[k]$ is implemented with the following recursive equation (Jimenez et al., 2004; Zhang, Wang, & Lu, 2011)

$$P[k] = \omega \left|r_{\mathrm{d}}[k]\right|^2 + (1-\omega)\, P[k-1] \ , \tag{5.11}$$

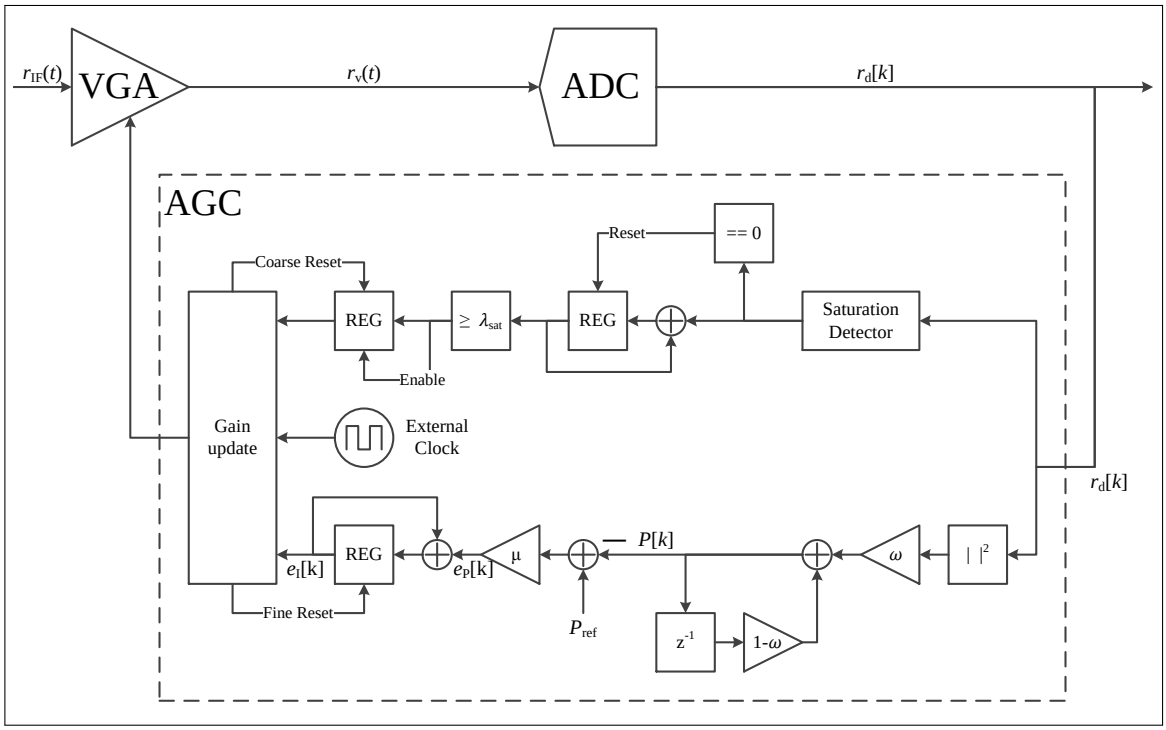

FIGURE 5.8. System structure of AGC.

where $0 \leq \omega \leq 1$ takes into account how much memory the estimator has. This LPF corresponds to a exponential moving average, which approximates a simple moving average of N_s samples by setting $\omega = \frac{N_s}{2}$ (Demosthenous, Nicolaou, & Georgiou, 2010).

The smoothed power signal is then compared to a reference P_{ref}, which produces an error signal

$$e_P[k] = \mu \left(P_{ref} - P[k] \right) \quad , \tag{5.12}$$

where $\mu \in \mathbb{R}^+$ is a constant. With an accumulator, this error is integrated as

$$e_I[k] = e_I[k-1] + e_P[k] \quad . \tag{5.13}$$

The Gain Update block takes the informations of both branches an makes a decision based on the state machine shown in Fig. 5.9.

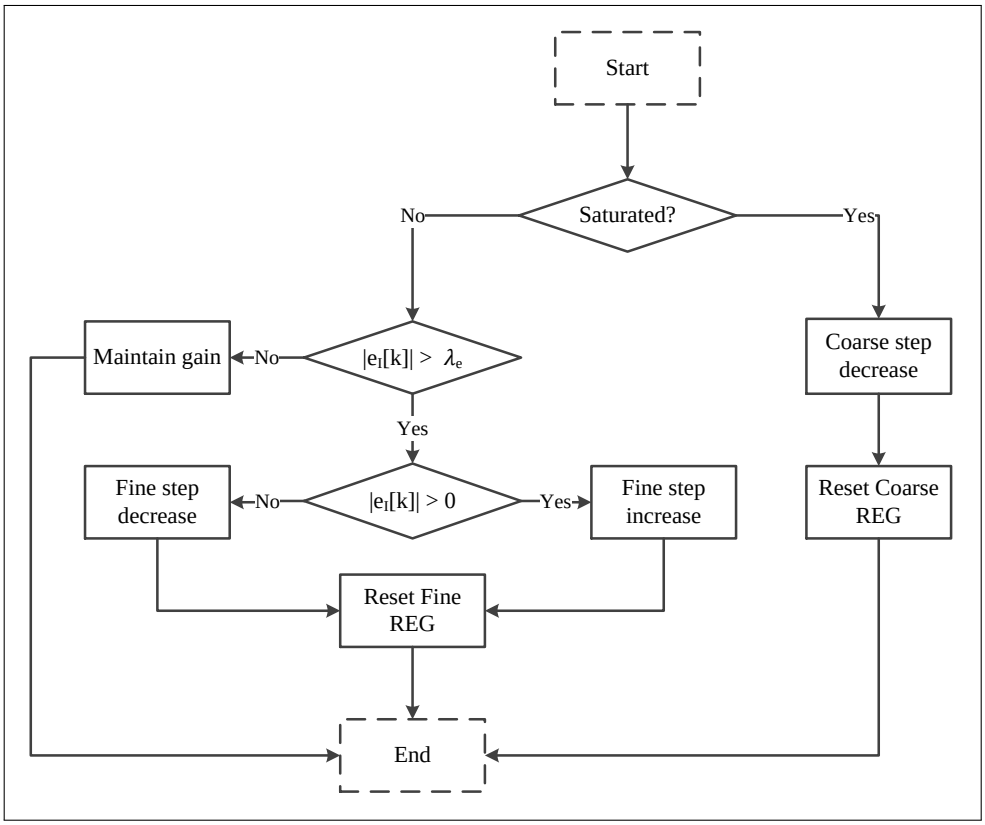

FIGURE 5.9. Gain update state machine.

The feedback from the digital AGC to the VGA has a certain latency, which makes impractical to update the gain at every sample. Hence, the state machine works with an external clock of lower frequency such that the decision is made at a rate $N_{\text{UR}} < N_{\text{up}}$ times the symbol rate. In this thesis, $N_{\text{UR}} = 32$, due to a limited transfer data rate between the baseband modem and the VGAs. The Gain Update block checks if there is a coarse action to be taken due to ADC saturation. If so, the gain is decreased by 3 dB and the coarse register is reset. If no coarse action flag was raised, then the magnitude of the accumulated error is checked. If the error is higher than a certain threshold λ_{e} the gain is increased or decreased (depending on the sign of the error) by a small given step of 0.2 dB. Otherwise, the gain is maintained.

5.2.2 Performance Validation

The settling time can be defined as the time it takes for the signal to reach a certain percentage range around the final value. In our case, we use the range of ± 3 dB of the final gain after the packet starts to be received. However, it turns out that the settling time does not depend only on the architecture, but also on the magnitude of the incoming the signal. As intuition suggests, the larger the incoming signal the longer the time needed to stabilize the VGA gain. Therefore, the settling time should be defined for the highest-gain reduction, which corresponds to 50 dB.

Simulations were performed to adjust the different parameters of the AGC to optimize the settling time. The simulations considered that the receiver is in an idle listening state, in which only thermal noise, at a room temperature (300 K), is processed by the AGC. Then, a packet (IF signal) with a given average SNR is received. An example of the received signal at the antenna, the VGA gain and the digital signal is shown in Fig. 5.10.

Monte Carlo simulations were performed in order to characterize the behavior of the AGC for a given average SNR. However, the actual SNR depends on the realization of a Rayleigh channel, which is randomly generated for each run as i.i.d circularly symmetrical complex Gaussian random variable with zero mean and unit variance. Fig. 5.11 shows the distribution of the settling time for a given IF signal, which is less than $4T_{\mathrm{s}}$ or 0.3 ms for more than 99.9 % of the cases with the maximum average SNR of 50 dB. For the SNR target of the PPP, i.e. less than 10 dB, the settling time is practically negligible.

5.3 Ping-Pong-Payload Performance in LATINA UC Simulator

This section describes the performance of the PPP scheme with the LATINA UC testbed specifications already presented. The simulations were performed considering $L_{\mathrm{a}} = L_{\mathrm{b}} = 32$, because this is the training length necessary for the synchronization tasks at the SNR of interest (Feres, 2013). The system was considered in a 4×4 MIMO configuration.

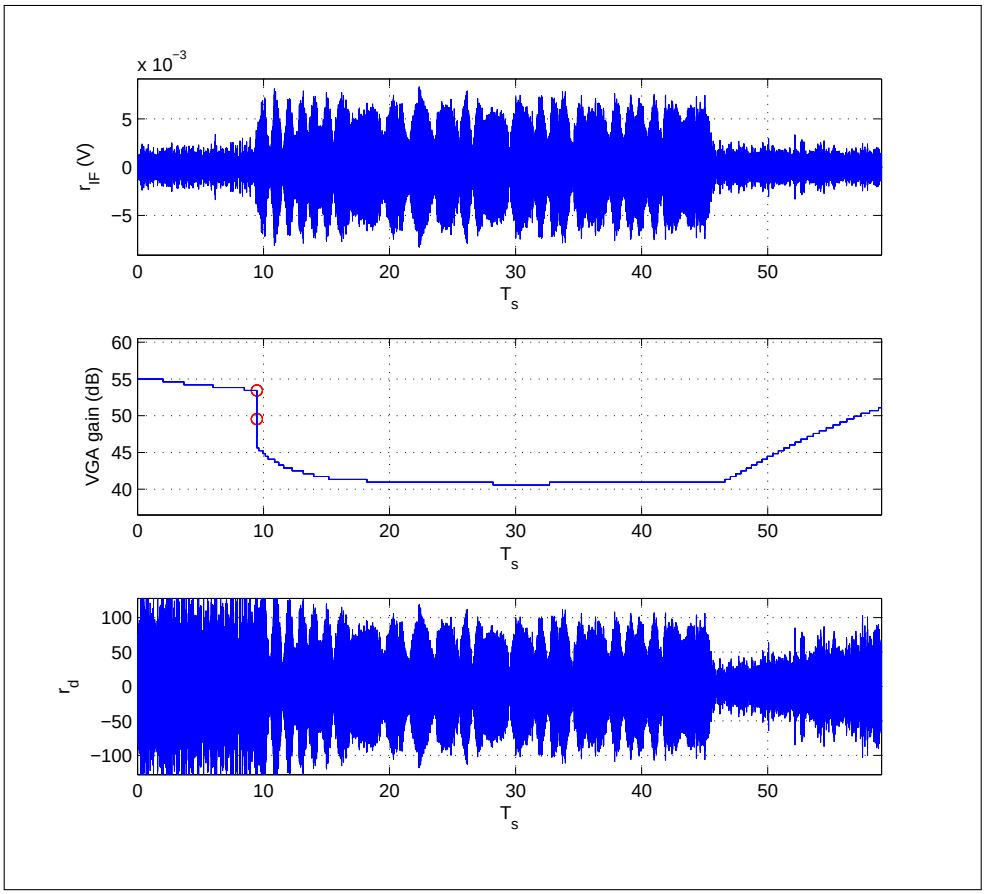

FIGURE 5.10. On the top, the IF signal before VGA action is depicted. On the center, the VGA gain which is applied to the IF signal is shown. The circles represent the times coarse action is performed. On the bottom, the digital signal is depicted.

Fig. 5.12 shows the BER for the ideal case of Chapter 4 and the simulations with the LATINA UC specifications. In Fig. 5.13 the losses respect to the ideal case can be seen. This suggests that the SNR loss can be as high as 1 dB due to real implementation considerations. The reason that the PPP suffers a larger deterioration than the MRC scheme can be explained by the AGC stabilization. PPP corresponds to a MIMO communication. Therefore, as explained in Section 5.1.2, the AGC has to be stabilized every time the transmit antenna changes. Conversely, in the MRC this process is performed only at the beginning of the packet.

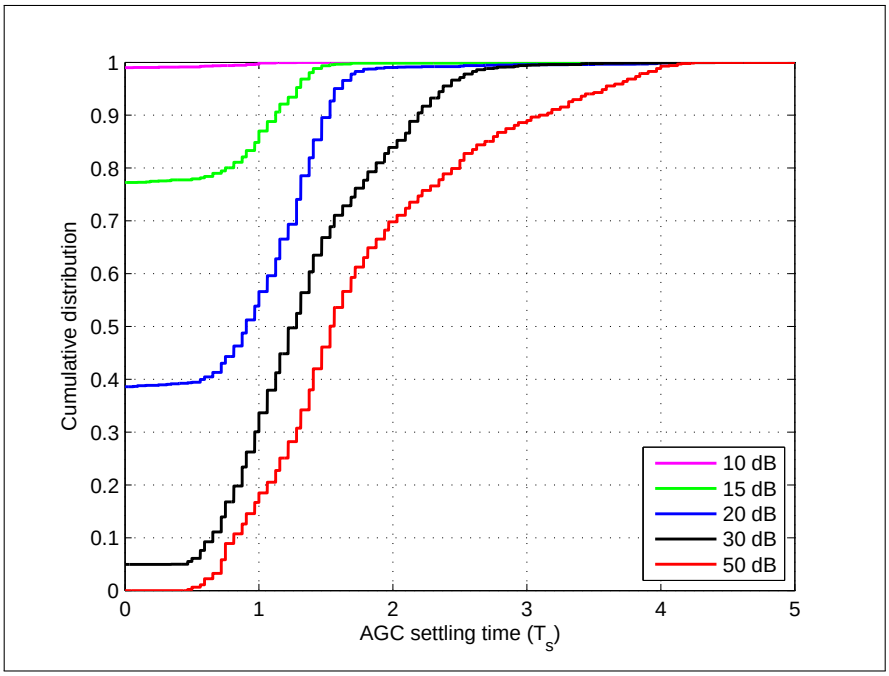

FIGURE 5.11. AGC settling time cumulative distribution for different SNRs.

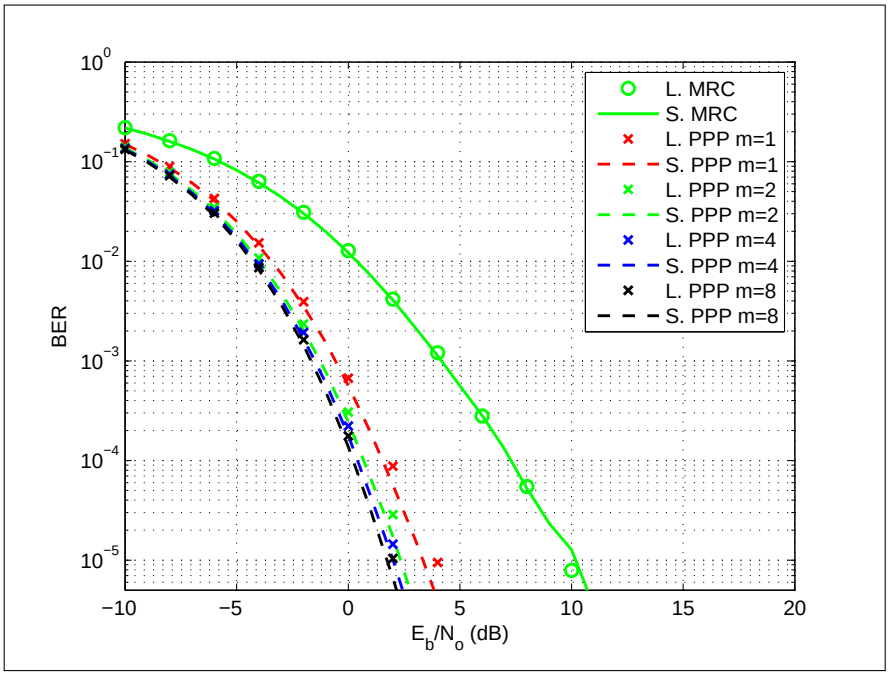

FIGURE 5.12. BER for simulations with LATINA testbed specifications and ideal case of Chapter 4 using a 4×4 MIMO configuration. L. stands for LATINA UC testbed and S. for the ideal simulations of Section 4.3

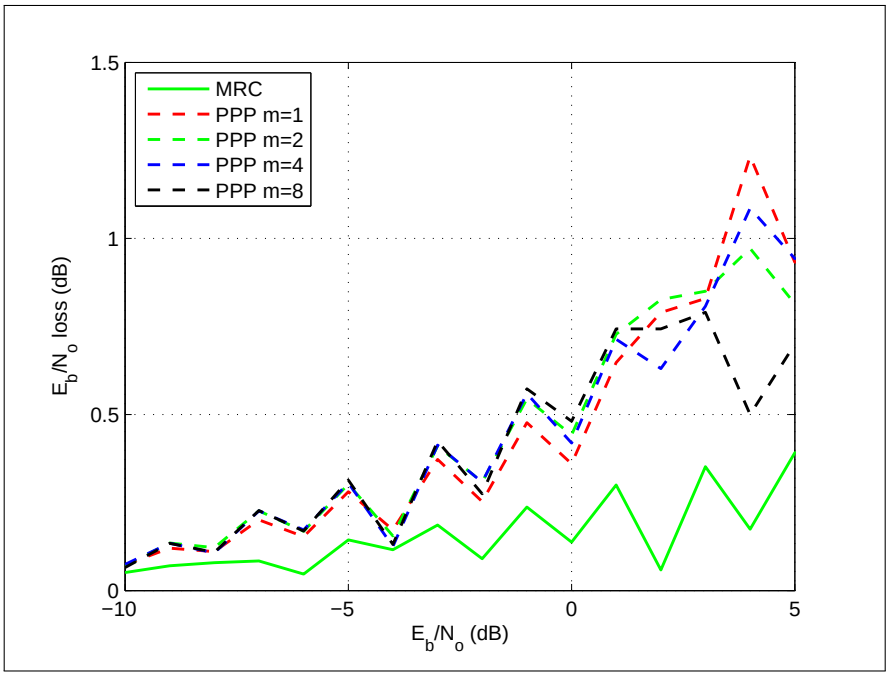

FIGURE 5.13. SNR losses of the PPP simulated with LATINA UC testbed specification respect to the ideal simulations of Section 4.3.

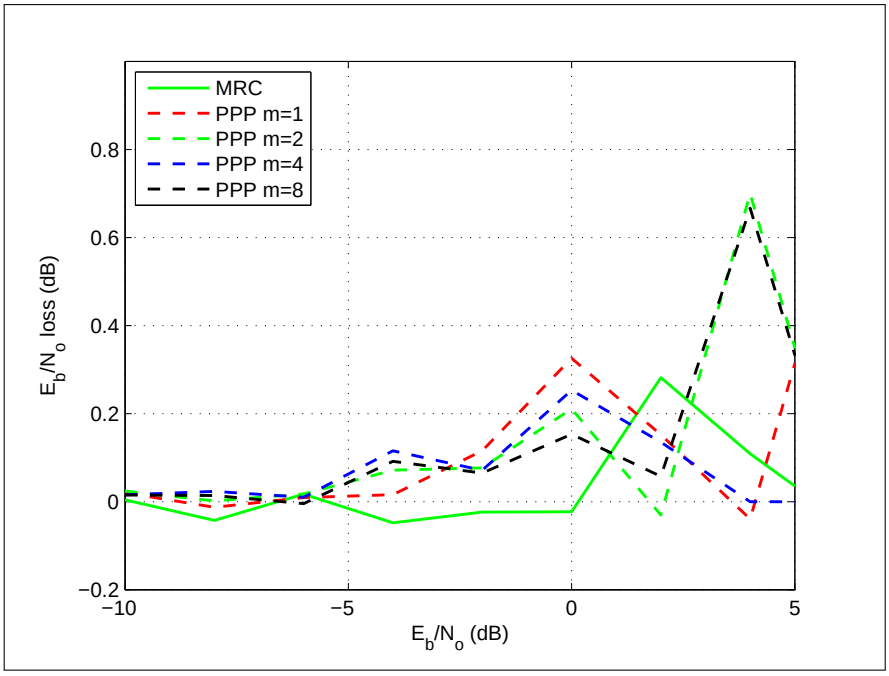

FIGURE 5.14. SNR losses due to distortion produced by the AGC on the channel estimates in the LATINA testbed simulator.

Since the AGC distortions explained in Section 5.1 are not easy to correct, due to the processing capacity limitations, we measured the performance loss. This mean, the effect of not dividing each channel matrix coefficient by its corresponding VGA gain. Fig. 5.14 represents the SNR loss produced by the AGC channel distortion. The results show that the performance loss is negligible. The reason can be found on the ratio $B_{\mathrm{W}}/B_{\mathrm{I}} \approx 20$ of the LATINA UC testbed, which as was shown in Fig. 5.7, produces performances losses of less than 1 dB.

The previous results suggest that given the specific conditions of the LATINA UC testbed, the correction of the distortions produced by the AGC may not be necessary considering the high-complexity operations that are required. However, this affirmation may change if the PPP scheme was to be implemented in a different platform.

6. CONCLUSIONS AND FUTURE WORK

6.1 Overall Conclusions

In this thesis we examined the problem of setting up a communication link over narrow-band quasi-static MIMO channels using SVD-based beamforming.

We proposed a method that, instead of relying on feeding back actual channel or SVD coefficients from receiver to transmitter, takes advantage of the channel reciprocity property to acquire the required precoding vector at the transmitter. The presented algorithm uses a 3-step preamble transmission with a first forward preamble transmission Ping used for channel training, then a backward response Pong for channel-dependent reverse channel training, and finally a forward Payload transmission that carries the actual payload data. The performance of the method depends on the quality of the channel estimates, and therefore different training preamble lengths were studied. As intuition suggests, as the preamble length grows the performance improves. However, the impact of each extra iteration on the BER seems to not depend much on the lengths.

This technique requires to attain knowledge, during the Ping stage, of the first singular vector, instead of the full SVD. In order to accomplish so, our technique comprises a low-complexity method for computing the necessary vector, which is based on the PIA. Furthermore, this iterative method also provides the flexibility to adjust the quality of the link by changing the number of iterations performed, not requiring to transmit more times as most of the solutions in the literature do for improving the performance. As simulations confirm, by only performing 3 iterations the results achieve a performance loss of less than 1 dB compared to the perfect SVD computed on the same channel estimate.

The proposed method can be slightly modified by re-estimating the decoding vector at the Payload stage. The results suggest that performing this extra estimation is almost equivalent to perform an extra iteration of the PIA during the Ping stage. In the case when $m = 1$ iteration, the SNR gain given by the re-estimation can be as high as 1 dB.

We studied acquisition considerations for implementing the PPP algorithm in real digital communication systems. This included synchronization tasks such as packet detection, timing recovery and CFO correction. An algorithm proposed in the literature was chosen for its compatibility with our scheme. Instead of transmitting a preamble for synchronization and a different one for channel estimation, a single preamble is used for both tasks. This joint solution allows to reduce the overhead for each transmission.

The study also comprises channel estimation deterioration due to AGC effects. The results show that in low SNR scenarios the performance improves as the SNR increases respect to the theoretical case, because the gain of the AGC is dominated by the effect of the thermal noise, whose power is relatively constant and independent of the transmit antenna. Conversely, at high SNR, the performance deteriorates with an increase of the SNR, as the AGC is dominated by the effect of the channel realizations, which are different for each transmit antenna.

Furthermore, hardware architecture considerations were analyzed. The study included the description of the most suitable transceiver architecture for a narrow-band quasi-static MIMO system. The LATINA UC testbed was presented and an digital AGC loop was developed for it.

Finally, the PPP method was simulated with the specifications of the testbed developed in LATINA UC. The results show that the proposed algorithm approaches the theoretical BER of the SVD-based beamforming, with an SNR loss that can be as high as 1 dB. Furthermore, results show that the distortion of the channel estimates are negligible for the SNR of interest given the noise bandwidth in effect at the ADC. The results suggest that correcting this distortion is not critical.

6.2 Future Work

This work focuses in developing a robust and low-complexity algorithm for setting up point to point SVD beamforming links. Nonetheless, communication networks are

composed by several nodes. Hence, some strategies have to be proposed to establish multi-user SVD beamforming links.

The ultimate goal of our proposal is to make an energy efficient link. This thesis proposes a way of establishing the SVD beamforming link such that the BER is close to the theoretical one. However, we would like to give an answer to the question: when is it convenient to use the PPP scheme for energy efficiency? In order to do that, a detailed analysis of energy has to be done, similar to the one done by Rosas and Oberli (2012a). This has to consider the RF electronic consumption, the energy consumption due to electromagnetic radiation, the energy spent by digital components in the processing of packets, and the energy for retransmissions if packets are detected wrongly.

References

Alegre, J., Celma, S., & Calvo, B. (2011). *Automatic Gain Control: Techniques and Architectures for RF Receivers*. Springer.

Bensky, A. (2004). *Short-range Wireless Communication: Fundamentals of RF System Design and Application*. Elsevier Science.

Besson, O., & Stoica, P. (2003, March). On parameter estimation of mimo flat-fading channels with frequency offsets. *Signal Processing, IEEE Transactions on*, *51*(3), 602-613.

Björck, A. (1996). *Numerical Methods for Least Squares Problems*. Society for Industrial and Applied Mathematics.

Crols, J., & Steyaert, M. (1998, Mar). Low-IF topologies for high-performance analog front ends of fully integrated receivers. *Circuits and Systems II: Analog and Digital Signal Processing, IEEE Transactions on*, *45*(3), 269-282.

Czylwik, A. (1999). Synchronization for systems with antenna diversity. In *Vehicular technology conference, 1999. vtc 1999 - fall. ieee vts 50th* (Vol. 2, p. 728-732 vol.2).

Dahl, T., Christophersen, N., & Gesbert, D. (2004, Sept). Blind MIMO eigenmode transmission based on the algebraic power method. *Signal Processing, IEEE Transactions on*, *52*(9), 2424-2431.

Demosthenous, P., Nicolaou, N., & Georgiou, J. (2010, Nov). A hardware-efficient low-pass filter design for biomedical applications. In *Biomedical circuits and systems conference (biocas), 2010 ieee* (p. 130-133).

Drentea, C. (2010). *Modern Communications Receiver Design and Technology*. Artech House.

Du, Q., Jiang, M., Lin, G., & Sun, N. (2003, April). All-digital AGC in CDMA base station receiver. In *Communication technology proceedings, 2003. icct 2003. international conference on* (Vol. 2, p. 1037-1041 vol.2).

Eckart, C., & Young, G. (1939, February). A principal axis transformation for non-Hermitian matrices. *Bull. Amer. Math. Soc.*, *45*(2), 118-121.

Feres, C. (2013). *Algoritmos de adquisición para redes inalámbricas de sensores con tecnología de múltiples antenas* (Unpublished master's thesis). Pontificia Universidad Católica de Chile.

Gazor, S., & AlSuhaili, K. (2010, July). Communications over the Best Singular Mode of a Reciprocal MIMO Channel. *Communications, IEEE Transactions on*, *58*(7), 1993-2001.

Goldsmith, A. (2005). *Wireless Communications*. Cambridge University Press.

Golub, G., & Kahan, W. (1965). Calculating the Singular Values and Pseudo-Inverse of a Matrix. *Journal of the Society for Industrial and Applied Mathematics: Series B, Numerical Analysis*, *2*(2), pp. 205–224.

Golub, G., & Reinsch, C. (1970). Singular value decomposition and least squares solutions. *Numerische Mathematik*, *14*(5), 403–420.

Golub, G., & Van Loan, C. (1996). *Matrix Computations (3rd Ed.)*. Baltimore, MD, USA: Johns Hopkins University Press.

Green, D. (1983, Feb). Global stability analysis of automatic gain control circuits. *Circuits and Systems, IEEE Transactions on*, *30*(2), 78-83.

Guillaud, M., Slock, D. T. M., & Knopp, R. (2005, August). A practical method for wireless channel reciprocity exploitation through relative calibration. In *Signal processing*

and its applications, 2005. proceedings of the eighth international symposium on (Vol. 1, p. 403-406).

Hassibi, B., & Hochwald, B. (2003, April). How much training is needed in multiple-antenna wireless links? *Information Theory, IEEE Transactions on*, *49*(4), 951-963.

Haustein, T., Jorswieck, E., Jungnickel, V., Krueger, U., Pohl, V., & Von Helmolt, C. (2001). Bit error rates for a MIMO system in Rayleigh and Rician channels. In *Vehicular Technology Conference, 2001. VTC 2001 Fall. IEEE VTS 54th* (Vol. 4, p. 1984-1987 vol.4).

Jimenez, V., Fernandez-Getino Garcia, M., Serrano, F., & Armada, A. (2004, Nov). Design and implementation of synchronization and AGC for OFDM-based WLAN receivers. *Consumer Electronics, IEEE Transactions on*, *50*(4), 1016-1025.

Jungnickel, V., Kruger, U., Istoc, G., Haustein, T., & Von Helmolt, C. (2004, June). A mimo system with reciprocal transceivers for the time-division duplex mode. In *Antennas and propagation society international symposium, 2004. ieee* (Vol. 2, p. 1267-1270 Vol.2).

Lee, I.-G., Son, J., Choi, E., & Lee, S.-K. (2006, May). Fast automatic gain control employing two compensation loop for high throughput MIMO-OFDM receivers. In *Circuits and systems, 2006. iscas 2006. proceedings. 2006 ieee international symposium on* (p. 4 pp.-).

Liang, L., Shi, J., Chen, L., & Xu, S. (2010, June). Implementation of Automatic Gain Control in OFDM digital receiver on FPGA. In *Computer design and applications (iccda), 2010 international conference on* (Vol. 4, p. V4-446-V4-449).

Liu, W., Li, X., & Chen, M. (2005, March). Energy efficiency of MIMO transmissions in wireless sensor networks with diversity and multiplexing gains. In *Acoustics, speech,*

and signal processing, 2005. proceedings. (icassp '05). ieee international conference on (Vol. 4, p. iv/897-iv/900 Vol. 4).

Love, D., Heath, R., & Strohmer, T. (2003, Oct). Grassmannian beamforming for multiple-input multiple-output wireless systems. *Information Theory, IEEE Transactions on*, *49*(10), 2735-2747.

Mengali, U., & D'Andrea, A. N. (1997). *Synchronization Techniques for Digital Receivers*. Springer.

Mukkavilli, K., Sabharwal, A., Erkip, E., & Aazhang, B. (2003, Oct). On beamforming with finite rate feedback in multiple-antenna systems. *Information Theory, IEEE Transactions on*, *49*(10), 2562-2579.

Muñoz, C., & Oberli, C. (2012). Energy-efficient estimation of a MIMO channel. *EURASIP Journal on Wireless Communications and Networking*, *2012*(1), 353.

Nagaraj, S., Khan, S., Schlegel, C., & Burnashev, M. (2006, Aug). On preamble detection in packet-based wireless networks. In *Spread spectrum techniques and applications, 2006 ieee ninth international symposium on* (p. 476-480).

Narula, A., Lopez, M., Trott, M., & Wornell, G. W. (1998, Oct). Efficient use of side information in multiple-antenna data transmission over fading channels. *Selected Areas in Communications, IEEE Journal on*, *16*(8), 1423-1436.

Paris, D. (1969). *Basic Electromagnetic Theory*. McGraw-Hill.

Perels, D., Burg, A., Haene, S., Felber, N., & Fichtner, W. (2008, July). An automatic gain controller for MIMO-OFDM WLAN systems. In *Circuits and systems for communications, 2008. eccsc 2008. 4th european conference on* (p. 246-251).

Perels, D., Studer, C., & Fichtner, W. (2007, May). Implementation of a low-complexity frame-start detection algorithm for mimo systems. In *Circuits and systems, 2007. iscas 2007. ieee international symposium on* (p. 1903-1906).

Rappaport, T. (2002). *Wireless communications: principles and practice*. Prentice Hall PTR.

Razavi, B. (1998, June). RF IC design challenges. In *Design automation conference, 1998. proceedings* (p. 408-413).

Rosas, F. (2012). *Energy efficient SVD MIMO computation.*

Rosas, F., & Oberli, C. (2012a, Sept). Energy-efficient MIMO SVD communications. In *Personal indoor and mobile radio communications (pimrc), 2012 ieee 23rd international symposium on* (p. 1588-1593).

Rosas, F., & Oberli, C. (2012b, December). Modulation and SNR Optimization for Achieving Energy-Efficient Communications over Short-Range Fading Channels. *Wireless Communications, IEEE Transactions on*, *11*(12), 4286-4295.

Rosas, F., & Oberli, C. (2013, April). Nakagami-m approximations for multiple-input multiple-output singular value decomposition transmissions. *Communications, IET*, *7*(6), 554-561.

Rosas, F., & Oberli, C. (in press). *Impact of the channel state information on the energy-efficiency of MIMO communications.*

S., Goldsmith, A., & Bahai, A. (2004, Aug). Energy-efficiency of MIMO and cooperative MIMO techniques in sensor networks. *Selected Areas in Communications, IEEE Journal on*, *22*(6), 1089-1098.

Saito, H., Kagami, O., Umehira, M., & Kado, Y. (2008, December). Wide area ubiquitous network: the network operator's view of a sensor network. *Communications Magazine, IEEE*, *46*(12), 112-120.

Schellmann, M., Jungnickel, V., & Von Helmolt, C. (2005, Sept). On the value of spatial diversity for the synchronisation in mimo-ofdm systems. In *Personal, indoor and mobile radio communications, 2005. pimrc 2005. ieee 16th international symposium on* (Vol. 1, p. 201-205).

Sibille, A., Oestges, C., & Zanella, A. (2010). *MIMO: From Theory to Implementation*. Elsevier Science.

Simoens, F., & Moeneclaey, M. (2006, June). reduced complexity data-aided and code-aided frequency offset estimation for flat-fading mimo channels. *Wireless Communications, IEEE Transactions on*, *5*(6), 1558-1567.

Sklar, B. (1997, Jul). Rayleigh fading channels in mobile digital communication systems .I. Characterization. *Communications Magazine, IEEE*, *35*(7), 90-100.

Smith, G. (2004, June). A direct derivation of a single-antenna reciprocity relation for the time domain. *Antennas and Propagation, IEEE Transactions on*, *52*(6), 1568-1577.

Studer, C., Blosch, P., Friedli, P., & Burg, A. (2007, Nov). Matrix Decomposition Architecture for MIMO Systems: Design and Implementation Trade-offs. In *Signals, systems and computers, 2007. acssc 2007. conference record of the forty-first asilomar conference on* (p. 1986-1990).

Tang, Y., Vucetic, B., & Li, Y. (2005, Jun). An iterative singular vectors estimation scheme for beamforming transmission and detection in MIMO systems. *Communications Letters, IEEE*, *9*(6), 505-507.

Tse, D., & Viswanath, P. (2005). *Fundamentals of Wireless Communication*. New York, NY, USA: Cambridge University Press.

Venkataramani, R., & Marzetta, T. L. (2003). Reciprocal Training and Scheduling Protocol for MIMO Systems. In *Proc. 41st annual allerton conf. communication, control, computing.*

Vucic, M., & Butorac, M. (2009, May). All-digital high-dynamic automatic gain control. In *Circuits and systems, 2009. iscas 2009. ieee international symposium on* (p. 1032-1035).

Walls, F., & Vig, J. R. (1995, July). Fundamental limits on the frequency stabilities of crystal oscillators. *Ultrasonics, Ferroelectrics and Frequency Control, IEEE Transactions on*, *42*(4), 576-589.

Wen, C., Zhang, Y., & Jiang, L. (2011, Sept). Design and implementation of fast convergence and large dynamic digital Automatic Gain Control. In *Communication technology (icct), 2011 ieee 13th international conference on* (p. 767-770).

Xia, P., & Giannakis, G. (2006, May). Design and analysis of transmit-beamforming based on limited-rate feedback. *Signal Processing, IEEE Transactions on*, *54*(5), 1853-1863.

Xia, P., Niu, H., Oh, J., & Ngo, C. (2008, Sept). Practical Antenna Training for Millimeter Wave MIMO Communication. In *Vehicular technology conference, 2008. vtc 2008-fall. ieee 68th* (p. 1-5).

Zhan, C.-Z., Chen, Y.-L., & Wu, A.-Y. (2012, June). Iterative Superlinear-Convergence SVD Beamforming Algorithm and VLSI Architecture for MIMO-OFDM Systems. *Signal Processing, IEEE Transactions on*, *60*(6), 3264-3277.

Zhang, H., Wang, G., & Lu, M. (2011, May). Analysis and implementation of digital automatic gain control for DAB baseband decoder. *Consumer Electronics, IEEE Transactions on*, *57*(2), 327-334.

APPENDIX A. POWER ITERATION ALGORITHM

To obtain $\mathbf{u}_1$ from a matrix $\mathbf{H}$, a power iteration method is performed based on the following expansion of the SVD of the matrix (Golub & Van Loan, 1996)

$$\mathbf{H} = \mathbf{U}\boldsymbol{\Sigma}\mathbf{V}^{\dagger} \ . \tag{A.1}$$

Defining the Wishart matrix $\mathbf{W} = \mathbf{H}\mathbf{H}^{\dagger}$ and using the expansion of the SVD of $\mathbf{H}$ we obtain

$$\begin{aligned} \mathbf{W} &= \mathbf{U}\boldsymbol{\Sigma}\mathbf{V}^{\dagger}\mathbf{V}\boldsymbol{\Sigma}\mathbf{U}^{\dagger} \\ &= \mathbf{U}\boldsymbol{\Sigma}^{2}\mathbf{U}^{\dagger} \ . \end{aligned} \tag{A.2}$$

Taking the m-th power of $\mathbf{W}$ we attain

$$\begin{aligned} \mathbf{W}^{m} &= \mathbf{U}\boldsymbol{\Sigma}^{2}\mathbf{U}^{\dagger}\mathbf{U}\boldsymbol{\Sigma}^{2}\mathbf{U}^{\dagger}\cdots\mathbf{U}\boldsymbol{\Sigma}^{2}\mathbf{U}^{\dagger} \\ &= \mathbf{U}\boldsymbol{\Sigma}^{2m}\mathbf{U}^{\dagger} \ . \end{aligned} \tag{A.3}$$

Defining a random unit vector $\mathbf{z}_0 \in \mathbb{C}^{N_{\mathrm{r}}}$, we can find its decomposition such that

$$\begin{aligned} \mathbf{z}_0 &= \tilde{\mathbf{z}}_{\mathrm{N}} + \tilde{\mathbf{z}}_{\mathrm{R}} \\ &= \tilde{\mathbf{z}}_{\mathrm{N}} + \sum_{k=1}^{\mathrm{rank}(\mathbf{H})} \alpha_k \mathbf{u}_k \ , \end{aligned} \tag{A.4}$$

where $\tilde{\mathbf{z}}_{\mathrm{N}}$ is a vector in the null space of $\mathbf{W}$, $\tilde{\mathbf{z}}_{\mathrm{R}}$ is a vector in the column space or range of $\mathbf{W}$, and $\alpha_i \in \mathbb{R}$ is the projection of $\mathbf{z}_0$ on the direction $\mathbf{u}_i$. Recalling the orthonormality of singular vectors

$$\begin{aligned}\mathbf{W}^m\mathbf{z}_0 &= \mathbf{W}^m\left(\tilde{\mathbf{z}}_{\mathrm{N}} + \sum_{k=1}^{\text{rank}(\mathbf{H})} \alpha_k \mathbf{u}_k\right) \\ &= \mathbf{W}^m\tilde{\mathbf{z}}_{\mathrm{N}} + \sum_{k=1}^{\text{rank}(\mathbf{H})} \alpha_k \mathbf{W}^m\mathbf{u}_k \ .\end{aligned} \tag{A.5}$$

By definition, $\mathbf{W}\tilde{\mathbf{z}}_{\mathrm{N}} = \mathbf{0}$. Hence

$$\begin{aligned}\mathbf{W}^m\mathbf{z}_0 &= \sum_{k=1}^{\text{rank}(\mathbf{H})} \alpha_k \mathbf{W}^m\mathbf{u}_k \\ &= \sum_{k=1}^{\text{rank}(\mathbf{H})} \alpha_k \mathbf{U}\boldsymbol{\Sigma}^{2m}\mathbf{U}^\dagger\mathbf{u}_k \\ &= \sum_{k=1}^{\text{rank}(\mathbf{H})} \alpha_k \mathbf{U}\boldsymbol{\Sigma}^{2m}\hat{\mathbf{e}}_k \\ &= \sum_{k=1}^{\text{rank}(\mathbf{H})} \alpha_k \sigma_k^{2m}\mathbf{U}\hat{\mathbf{e}}_k \\ &= \sum_{k=1}^{\text{rank}(\mathbf{H})} \alpha_k \sigma_k^{2m}\mathbf{u}_k \ ,\end{aligned} \tag{A.6}$$

where $\hat{\mathbf{e}}_k$ is the k-th vector of the canonical basis.

Given that $\alpha_1 \neq 0$ with likelihood 1 and noting that as m increases $\frac{\sigma_k^{2m}}{\sigma_1^{2m}}$ tends to 0 $\forall k = 2, \cdots, \text{rank}(\mathbf{H})$, we obtain

$$\lim_{m\to\infty} \mathbf{W}^m\mathbf{z}_0 = \alpha_1\sigma_1^{2m}\mathbf{u}_1 \ . \tag{A.7}$$

Dividing the previous expression by its norm, the result is

$$\lim_{m\to\infty} \frac{\mathbf{W}^m\mathbf{z}_0}{||\mathbf{W}^m\mathbf{z}_0||} = \mathbf{u}_1 \ . \tag{A.8}$$